Review | Open Access

Energy Z

Yang *et al. Energy Z* **2026**, *2*, 200010 **DOI:**10.20517/energyz.2026.15

Heterostructures for advanced rechargeable batteries

Zheng Yang[1,#], Wenlu Yuan[1,#], Tao Wang[1,*], Kenneth I. Ozoemena[2], Svetlana Eliseeva[3], Yuping Wu[1,*]

Keywords:
Heterostructure, Li/Na/K-ion batteries, lithium-sulfur battery, metal-air battery, aqueous battery

Citation: Yang, Z.; Yuan, W.; Wang, T.; Ozoemena, K. I.; Eliseeva, S.; Wu, Y. Heterostructures for advanced rechargeable batteries. *Energy Z* **2026**, *2*, 200010. https://dx.doi.org/10.20517/energyz.2026.15

Received: 7 Apr 2026
First Decision: 28 Apr 2026
Revised: 29 Apr 2026
Accepted: 30 Apr 2026
Published: 17 Jun 2026

Academic Editor:
Jianyu Huang
Copy Editor:
Shu-Yuan Duan
Production Editor:
Shu-Yuan Duan

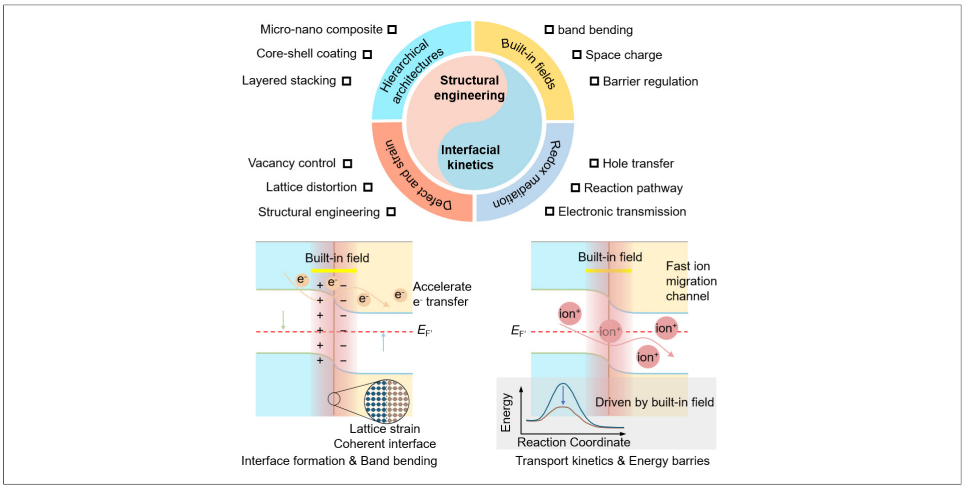

Abstract

Heterostructure materials with well-defined interfaces between distinct materials generate key interfacial physical effects, including band bending, built-in electric fields, and lattice strain. An inferior heterointerface severely hinders ion transport across the interface and exacerbates interfacial side reactions, leading to a shorter battery cycle life. In this review, we systematically examine the design principles and functional mechanisms of heterostructures for rechargeable batteries. The fundamental properties of heterostructures can be categorized into built-in electric fields that accelerate charge transfer, catalytic activity arising from interfacial defects, and the buffering effect of rigid-flexible coupled structures. We further summarize the latest advancements in heterostructures to mitigate electrode phase transitions and volume expansion in metal-ion batteries, including the realization of catalytic conversion of lithium polysulfides in lithium-sulfur batteries, the reduction of overpotential for oxygen reactions at the Mott-Schottky interface in metal-air batteries, and the inhibition of hydrogen evolution in aqueous batteries. This review aims to provide guidance for the rational design of

[1]Confucius Energy Storage Lab, School of Energy and Environment & Z Energy Storage Center, Southeast University, Nanjing 211189, Jiangsu, China.
[2]Molecular Sciences Institute, School of Chemistry, University of the Witwatersrand, Wits, 2050, Johannesburg, South Africa.
[3]Department of Electrochemistry, Institute of Chemistry, Saint Petersburg State University, St. Petersburg 199034, Russia.
[#]These authors contributed equally to this work.

[*]**Correspondence to:** Prof. Yuping Wu, Prof. Tao Wang, Confucius Energy Storage Lab, School of Energy and Environment & Z Energy Storage Center, Southeast University, Nanjing 211189, Jiangsu, China. E-mail: wangtao2021@seu.edu.cn; wuyp@seu.edu.cn

heterostructure electrodes in advanced rechargeable batteries, shifting strategies from empirical material combinations toward targeted interfacial functionality.

INTRODUCTION

Current rechargeable battery systems face critical challenges stemming from both electrode and electrolyte materials. For instance, the electrode materials of commercial lithium-ion batteries (LIBs) are constrained by the scarcity of transition-metal resources and rising costs, which are approaching the theoretical limit of energy density[1-3]. Moreover, the risk of thermal runaway caused by the decomposition of organic electrolytes at high voltage remains an unresolved safety concern[4-6]. Even though new types of rechargeable batteries attempt to leverage resource abundance, issues such as sluggish electrode kinetics and complex interfacial side reactions still hinder the simultaneous optimization of cycling stability and rate capability. These challenges not only reflect the limitations of single-component optimization, but also highlight the importance of investigating the fundamental coupling between interfacial charge transfer and structural stability. Therefore, the composite structure of the active materials and the interface engineering strategies deserve in-depth exploration.

Heterostructures are composite constructs formed by the interface between two or more materials with different physical and chemical properties[7]. They offer a promising route to surpass current material performance ceilings due to their unique capabilities in regulating interfacial electric fields, accelerating ion transport, and buffering volume strain[8]. The defining characteristics include interfacial band bending, built-in electric fields, and synergistic effects[9,10]. In rechargeable batteries, the advantages of heterostructures manifest in three aspects. Firstly, the charge transfer at the interface can be accelerated, and the polarization can be reduced. Secondly, stability of the interface can suppress side reactions. Thirdly, lattice defects induced by lattice mismatch can tune the adsorption energy of reaction intermediates[11-13]. The heterointerface thus enables synergistic enhancement of structure and dynamics.

This review focuses on heterostructures for advanced rechargeable batteries, including Li/Na/K-ion batteries, lithium-sulfur batteries (LSBs), metal-air batteries, and aqueous batteries. The role of heterostructures in addressing essential issues, including high ion diffusion barriers, lithium polysulfides (LiPSs) shuttling, excessive overpotential for oxygen reactions, and hydrogen evolution side reactions, is examined for different batteries. The construction strategies, interface action mechanisms, and electrochemical performance optimization paths of heterostructures in advanced rechargeable batteries are systematically reviewed. Furthermore, the challenges related to rational design and controllable synthesis of heterostructures are summarized. This review aims to lay the foundation for the design of heterostructure materials for next-generation advanced batteries.

BASIC PROPERTIES OF HETEROSTRUCTURES

Fundamental natures of heterostructures

Heterostructure materials integrate high-conductivity and high-stability components at the atomic scale, endowing the interfaces with multiple roles (such as electron conduction, ion transport, and stress buffering). Heterointerfaces often exhibit complex interfacial coupling effects due to inherent differences in Fermi levels, band structures, and lattice constants, with the most notable feature being the spontaneous formation of electric fields at the interface. Figure 1A illustrates the formation principle of a typical p-n junction. The p-type side contains more holes, and the n-type side contains more electrons. Electrons and holes migrate at the interface until the Fermi levels reach equilibrium. Figure 1B further shows the formation process of a heterointerface between two materials with different work functions. Upon contact, electrons spontaneously flow from the side with the lower work function to the side with the higher work function,

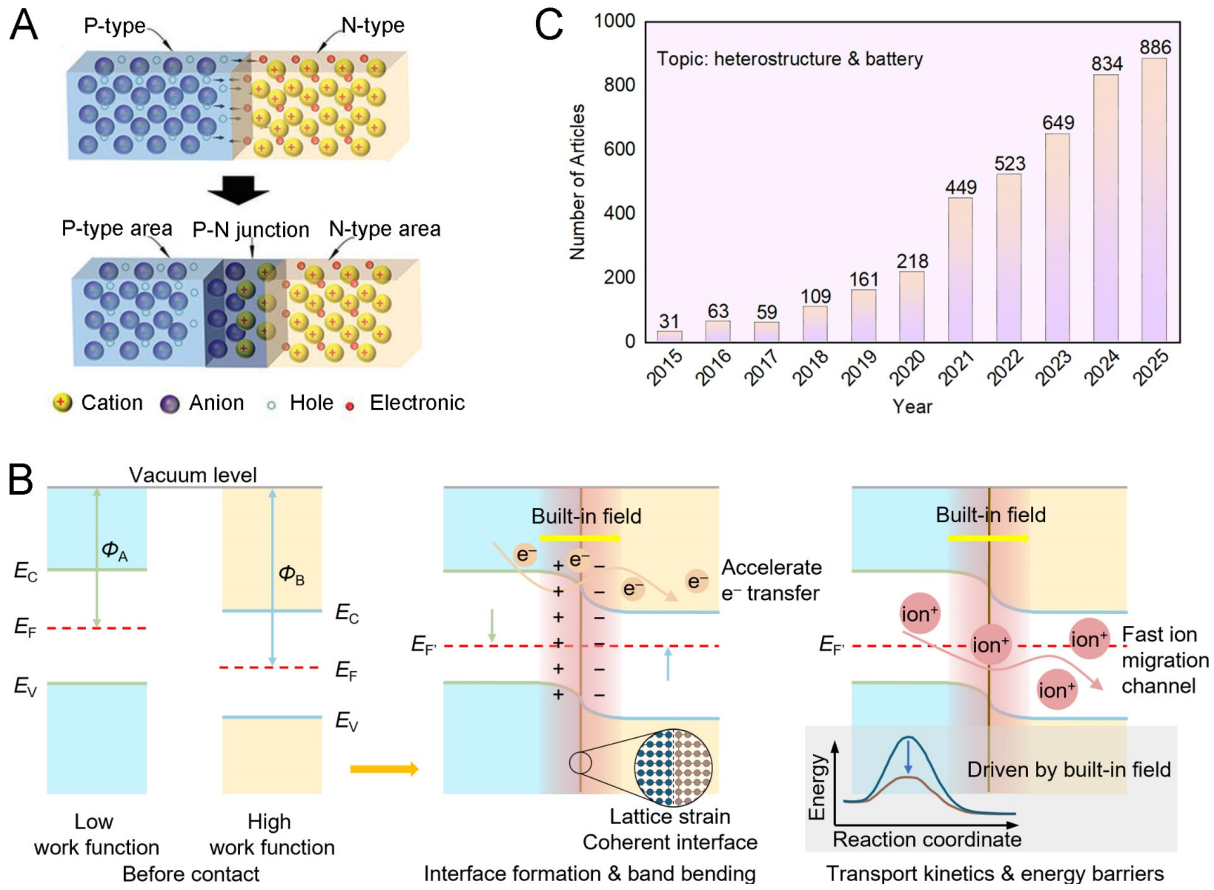

Figure 1. (A) Schematic illustration of p-n junction formation. (A) is reprinted with permission from Ref.[15], Copyright © 2022 Wiley; (B) Schematic illustration of the mechanism of heterointerface; (C) Number of articles dedicated to heterostructures in batteries. Database: Web of Science (https://webofscience.clarivate.cn).

leading to band bending and simultaneous generation of an electric field. This field not only provides the driving force and highly efficient charge-transfer pathways for ion/electron transport, but also endows the interface with rich cooperative catalytic active sites. The introduction of heterostructures into rechargeable batteries is critical for breaking through the kinetic limitations and enhancing structural stability of electrode materials.

Constructing an appropriate heterointerface is beneficial for accelerating charge transfer and buffering the volume expansion of active materials. In addition, optimizing the pathways and energy barriers of multiphase reactions (e.g., oxygen redox and sulfur conversion) enhances the rate performance, cycling stability, and energy efficiency of batteries[14]. The constituent materials that form a heterostructure often differ in their physical and chemical properties, such as work functions, lattice parameters, and ion-diffusion barriers. The judicious matching of these distinct parameters enables precise control over charge transfer and structural stability of the electrode material. In recent years, research on heterostructures for batteries has flourished [Figure 1C].

Built-in electric fields effect

Built-in electric fields originate from interfacial charge redistribution driven by differences in work function. When the direction of the built-in electric fields aligns with that of ion diffusion, the ion diffusion barrier can be significantly reduced. Meanwhile, a space charge layer forms at the interface, which alters the local ion concentration distribution and enhances the ion diffusion coefficient[6-8]. The ion concentration in the

space-charge layer follows the Poisson-Boltzmann equation. The ratio of interfacial conductivity to bulk conductivity can reach 10^2-10^3. For example, in the Mo_2C/MoO_3 heterostructure, the ratio can be 240 at 300 K and remains above 50 at 230 K, demonstrating that the built-in electric fields significantly promote ion transport even at low temperatures[16]. In the MXene/ZnTe heterostructure, the built-in electric fields raise the adsorption energy of K^+ and reduce the migration barrier[17]. In conversion-type materials and alloy anodes, the built-in electric fields accelerate electron migration from the current collector to the active materials and promote ion desolvation, thereby significantly reducing ohmic and electrochemical polarization[18]. In addition, the space charge layer often modifies the local concentration and migration energy barrier of ions. This reduces the diffusion barrier of Li^+ at the interface by an order of magnitude compared to the bulk phase[19]. The effective range of the built-in electric fields is limited by the Debye length (λ_D). When the characteristic size (d) of the heterostructures approaches or is smaller than λ_D, band bending extends throughout the entire particle, leading to bulk polarization. Indeed, a properly designed d/λ_D ratio can optimize the built-in electric field's effectiveness in promoting ion migration.

Lattice strain and defect concentration

When two materials with different lattice constants form an atomic-scale heterointerface, lattice distortion occurs to maintain atomic continuity. This generates lattice strain that directly alters bond lengths and bond angles, thereby influencing the band structure and *d*-band center of the material. These undercoordinated atomic configurations often act as highly active sites for electrochemical reactions, which exhibit a similar electrocatalytic effect for multi-electron reactions and effectively lower the reaction energy barrier. The $Ni\text{-}MoO_2/NiMoO_{4-x}$ optimizes the electronic structure by enriching nickel defect sites and utilizing the strain effect induced by the defects. This significantly reduces the adsorption energy barrier of hydrogen/oxygen intermediates in metal-air batteries[20]. The interfacial lattice mismatch δ is approximately 2.1%, corresponding to a strain energy of about 0.34 J m^{-2}. This strain energy can absorb approximately 16% of the volume-expansion work, thereby improving capacity retention from 42% for pristine MoO_3 to 89% after 300 cycles. The linear correlation between strain and capacity (R^2 = 0.93) indicates that strain exerts a dominant structure-buffering effect. The heterointerface also serves as a thermodynamically preferred site for defect formation, which realizes modulation of the electrochemical performance[21]. Defect-rich regions exhibit stronger chemical adsorption for LiPSs and effectively suppress their shuttle effect. Consequently, heterostructures not only provide electron/ion transport channels but also optimize the kinetic pathways of electrode reactions through defect engineering.

Interface buffering effect

To accommodate the volume changes during the charging/discharging of high-capacity materials, an interfacial buffering mechanism has been established. The combination of the "hard" components (such as carbon frameworks and inert oxides) and the "active" components in the heterostructures forms a 3D confinement effect and serves as an elastic buffer layer, which can prevent the agglomeration and pulverization of active materials and extend the cycle life[22]. When the active materials undergo volume expansion, the interface absorbs part of the strain energy through lattice slip or interface reconfiguration and naturally inhibits crack initiation and propagation[23]. Furthermore, the rigid components serve as the structural framework to maintain the mechanical integrity of the electrode as a whole. In summary, the interfacial buffering effect is crucial for cycling stability. Experimental results have proven that the capacity retention of heterostructure electrodes is substantially higher than that of single active materials.

THE ADVANTAGES OF HETEROSTRUCTURES

The core features of heterostructure materials can be categorized into structural engineering and interfacial kinetics, which together govern the overall electrochemical performance in batteries [Figure 2]. Structural engineering mainly focuses on the physical architecture of the heterointerface. At its core, the electronic state

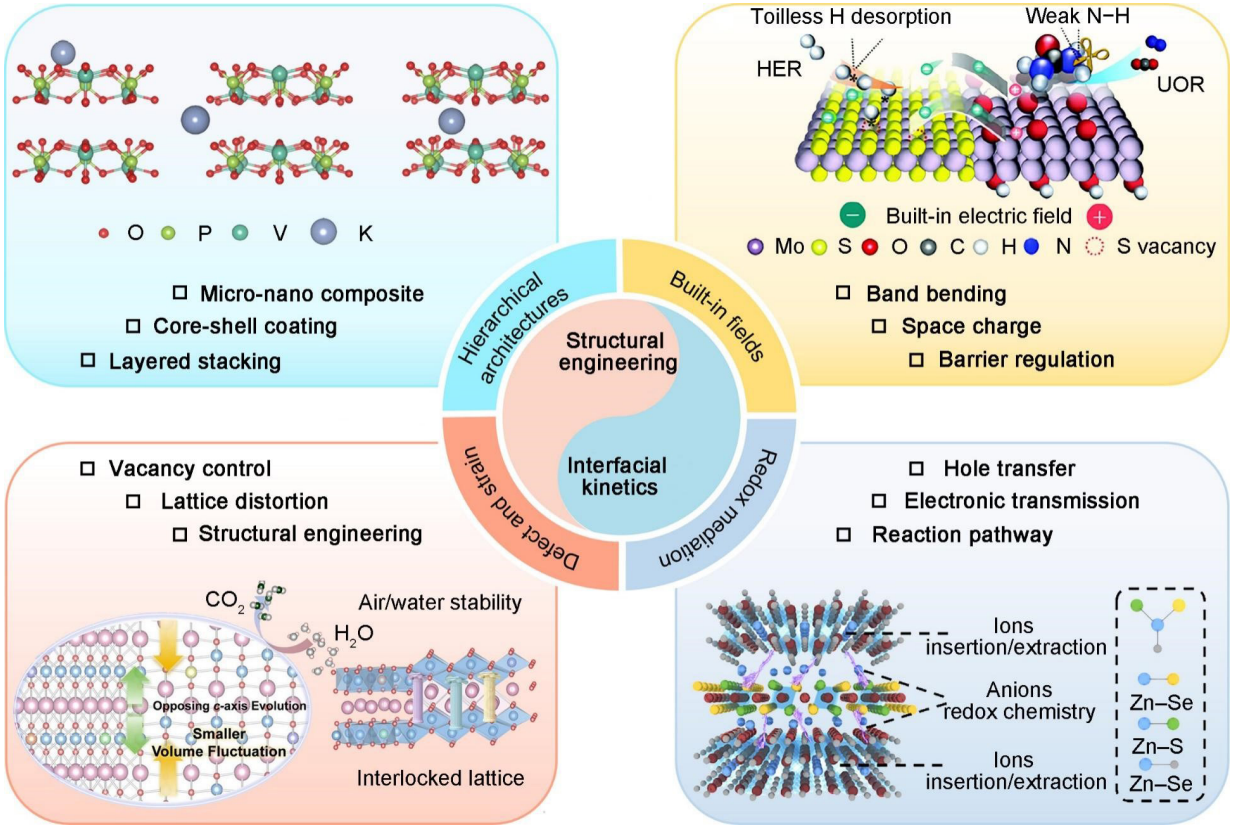

Figure 2. Schematic diagram of fundamental characteristics and functional mechanisms of heterostructures in rechargeable batteries. Hierarchical architectures[24], under CC BY 4.0 license; Defect and strain[25], reprinted with permission, Copyright © 2025 Wiley; Redox mediation[26], reprinted with permission, Copyright © 2025 Wiley; Built-in fields[27], under CC BY 4.0 license. HER: Hydrogen evolution reaction; UOR: urea oxidation reaction.

reconstruction and mechanical response at the interface are correlated through a common atomic-scale mechanism, which offers a stress-buffering strategy that transcends any single design approach. This is achieved through several structural engineering strategies. Layered stacking expands interlayer spacing and facilitates rapid ion intercalation[24]. Core-shell coatings protect active materials from electrolyte corrosion while improving air and water stability. Micro-nano composite structures shorten ion diffusion pathways and provide mechanical support. In addition, vacancy engineering and lattice distortion create additional active sites and alleviate volume fluctuation[25]. Interlocked lattice configurations suppress interlayer slip and mitigate structural deformation, whereas doped intercalation activates multi-anionic redox chemistry to provide extra capacity[26]. In contrast, interfacial kinetics mainly govern the charge-transfer dynamics and reaction pathways at the heterointerface. The key kinetic advantages include electric fields driving the adsorption/desorption of reaction intermediates with high catalytic activity[27], energy barrier regulation, optimized charge transport enabled by space-charge effects and band alignment, and steering reaction pathways of intermediates such as LiPSs toward favorable conversion[28]. Ultimately, the synergistic combination of structural engineering and interfacial kinetics enables heterostructures to achieve breakthroughs in capacity, cycle life, rate capability, and application.

Generally, a well-designed heterostructure should exhibit advantages across several interrelated aspects[29-31]. Firstly, they harness built-in electric fields and space-charge layers to promote fast charge separation and low-barrier ion migration in terms of electronic and ionic transport, which simultaneously activates multiple redox couples and realizes high energy density. Secondly, the heterostructures employ lattice distortion, vacancy control, and micro-nano composite architectures to buffer volume expansion with respect to

structural mechanics and volumetric stability. Thirdly, heterostructures optimize the adsorption/desorption behavior of key intermediates and reduce reaction overpotentials through barrier regulation and space-charge effects, and facilitate multi-electron transfer via orbital hybridization and spin polarization. Fourthly, to ensure environmental stability and practicality, the heterostructures can incorporate densely bonded atomic interfaces to suppress residual alkali formation and metal dissolution. These mechanisms are highly interconnected and mutually reinforcing. In summary, their synergistic integration constitutes the theoretical foundation that enables heterostructures to overcome the performance bottlenecks of traditional single-phase materials.

Regulation of reaction kinetics

The built-in electric fields significantly reduce the activation energy of charge transfer and promote the directional transport of electrons from the low-conductivity active materials to high-conductivity components. For instance, the band gap of the composite electrode is significantly reduced compared to that of the single electrode in $ZnCo_2O_4/SnO_2$[32], which greatly improves electron transport efficiency. Furthermore, the electric fields accelerate electron transport and increase ionic migration channels in MoB/Si_3N_4[33]. For MXene-based heterostructures, $Ti_3C_2T_x$ has a high electronic conductivity similar to metals (up to ~ 8,000 S cm^{-1}), and it can be combined with active materials such as transition metal sulfides or metal-organic frameworks to construct a continuous 3D conductive network[34], which effectively overcomes the insufficient conductivity.

Interfacial built-in fields

The heterointerface, which serves as an ion transport channel, converts conventional solid-phase diffusion into rapid interface-dominated migration. This is especially significant for potassium-ion batteries (PIBs) due to the large ionic radius of K^+ (1.38 Å)[35]. The heterointerface in $NiTe_2/MoS_2$ was also reported to reduce the diffusion energy barrier for K^+[36]. Moreover, Zhang *et al.* reported that the enhanced built-in electric fields at the heterointerface not only promote electron transmission but also accelerate the directional migration of Li^+[37], which demonstrated the lowest Li^+ diffusion impedance during cycling.

Reaction pathway optimization

The effectiveness of heterostructures in electrochemical reaction kinetics stems primarily from the regulation of reaction pathways. Heterointerfaces can induce uniform nucleation and the growth of discharge products for electrodes in conversion reactions, which prevents the formation of large insulating crystal domains and improves the reaction reversibility. In LSBs, the MoO_2 and N-deficient carbon nitride (MoO_2/DCN) catalyst can adsorb LiPSs with an adsorption energy of –4.85 eV, which is much higher than that of a single DCN (1.15 eV), thus effectively suppressing the shuttle effect[38]. *In-situ* ultraviolet visible (UV-vis) spectroscopy tests indicate that the heterostructures generate more S_3^- free radicals during discharge, with faster conversion rates of Li_2S_8 and Li_2S_6, and more thorough solid-liquid conversion, which can consequently improve sulfur utilization and cycling stability[39].

Structural buffering effect

Numerous conversion-reaction-based electrode materials undergo volume changes even exceeding 300%, and the mechanical stress will lead to the pulverization and failure of the active materials[40]. Through integrating two or more materials with distinct mechanical properties and crystal structures at the nanoscale to form heterostructures, stress-dissipation and buffering zones are created at the interfaces to effectively mitigate volume strain. For example, in a CoS_2/Co heterostructure, the ordered checkerboard-like architecture provides sufficient space to accommodate volume changes, delivering a capacity retention of 900 mAh g^{-1} with high S loading of 7.13 mg cm^{-2} and a low E/S ratio of 4.5 mL g^{-1}[41]. In the Si_3N_4/MoB@GO sandwich heterostructure, the introduction of the graphene intermediate layer not only improves

conductivity, but also buffers volume changes and provides excellent structural stability[42]. Moreover, chemical bonding and electrostatic forces at the heterointerface can further enhance the stability of the structure and inhibit interface degradation during long-term cycling.

Synergistic interfacial effects

The built-in electric fields in heterostructures can not only accelerate the interfacial migration of electrons and ions but also promote synergistic interfacial effects. Particularly, 2D/2D vertical stacking or 3D conductive framework-loaded heterostructures are beneficial for preventing the agglomeration and rearrangement of nanomaterials, which can generate a stronger synergistic effect through interfacial coupling[43]. Firstly, the high conductivity components are combined with the high capacity components, and it helps to achieve a balance between rate and capacity. Secondly, interface defects and dangling bonds provide additional active sites, which can enhance the pseudocapacitive contribution[44,45]. Thirdly, the combined action of multiple components promotes multi-electron reactions and contributes to high capacity. Finally, the design of heterostructures can improve battery safety and reduce potential hazards.

THE APPLICATIONS OF HETEROSTRUCTURES IN ADVANCED RECHARGEABLE BATTERIES

Metal-ion batteries

Metal-ion batteries operate on the "rocking-chair" principle, wherein metal ions reversibly intercalate and deintercalate between electrodes during charging/discharging, thereby converting electrical and chemical energy via redox reactions[46]. Solid-state diffusion in the electrodes and structural stability constitute the rate-limiting steps that dictate the energy output and cycle life of the battery[47]. Li-rich layered oxides (LLOs) are widely employed as cathodes for LIBs owing to their high specific capacity. However, they suffer from severe structural degradation caused by the out-of-plane migration of transition metals (TMs) from the TM layers to the alkali metal layers, and this process is further exacerbated by the formation of vacancy clusters and O-O dimers upon deep delithiation. To address this, Wang *et al.* designed an O2/O3 biphasic heterostructure consisting of a non-Li-rich O2 phase and a Li-rich O3 phase[48]. The heterointerface features a face-shared configuration and provides a strong electrostatic repulsion that can suppress the out-of-plane migration of TM ions from the Li-rich O3 domains. Simultaneously, the absence of Li vacancies in the TM layers of the non-Li-rich O2 phase further reduces the source of vacancies. This synergistic effect minimizes the formation of vacancy clusters and prevents the generation of detrimental O-O dimers, thereby stabilizing the anionic redox chemistry and preserving the integrity of lattice oxygen. Furthermore, $LiZr_2(PO_4)_3$ (LZP) was reported as a coating for LLOs to form an LLO/LZP heterostructure[49] [Figure 3A], which modulates the antibonding and O 2*p* non-bonding bands in LLOs [Figure 3B]. This modulation enhances Li^+ migration and electron transfer while suppressing irreversible phase transitions and side reactions. Owing to the enhanced lattice oxygen stability provided by the LZP layer, the generation of O_2 and CO_2 is reduced, and voltage decay is also alleviated.

Silicon anodes possess a high theoretical capacity of 4,200 mAh g^{-1} but suffer from a volume change of ~ 300% during cycling[52]. Zhu *et al.* developed a highly stable Si/$MoSe_2$@C heterostructure that reconciles the high capacity with superior stability[50] [Figure 3C]. Lattice-matched $MoSe_2$ bridges the porous silicon and carbon coating through covalent bonds to form stable Si-Se-Mo linkages that optimize Li^+ transport pathways and stabilize the structure. In this heterostructure, $MoSe_2$ serves as an electron-conductive and ion-permeable interlayer [Figure 3D] to reduce the maximum Li^+ migration energy barrier from 0.81 eV (Si@C) to 0.61 eV (Si/$MoSe_2$@C). Moreover, thermal conductivity measurements demonstrate that the heterointerface in Si/$MoSe_2$@C reduces interfacial thermal resistance, which results in a 27% increase in thermal conductivity [Figure 3E].

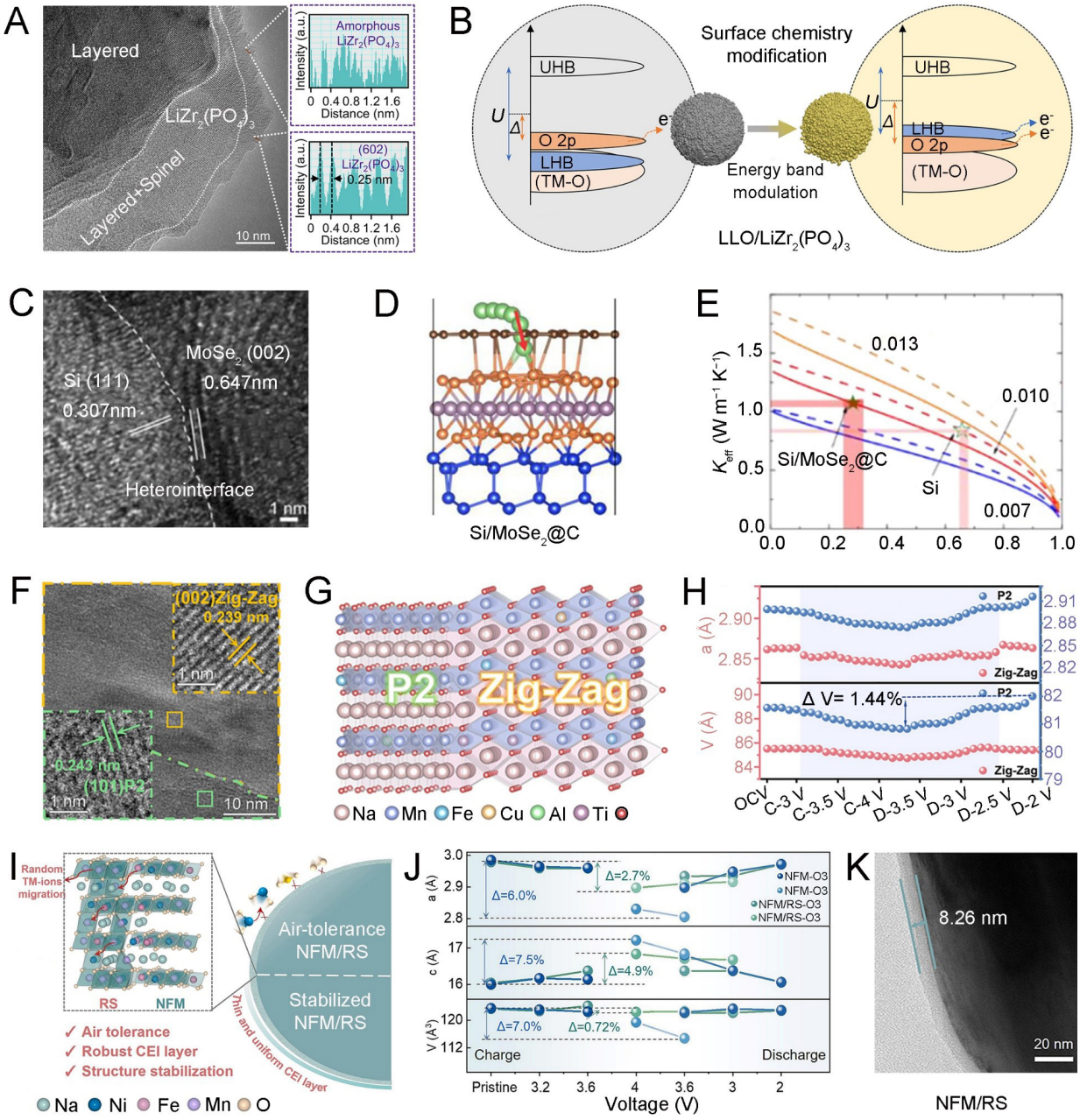

Figure 3. (A) High-resolution transmission electron microscope (HRTEM) image of LLO/LZP with FFT patterns; (B) Schematic illustration of energy band modulation through surface chemistry modification of LLO/LZP. (A and B) are reprinted with permission from Ref.[49], Copyright © 2025 Elsevier; (C) HRTEM image of the Si/$MoSe_2$@C heterostructure; (D) Optimized atomic structure in side view with overlaid Li^+ diffusion trajectories; (E) K_{eff} of Si and Si/$MoSe_2$@C-based matrix as a function of porosity (ε). (C-E) are reprinted from Ref.[50], under CC BY 4.0 license; (F) HRTEM image with insets showing magnified views of Zig-Zag and P2; (G) Schematic illustration of the P2/Zig-Zag heterostructure with atomic interlocking; (H) Lattice parameter evolution derived from XRD of the P2/Zig-Zag heterostructure. (F-H) are reprinted with permission from Ref.[25], Copyright © 2025 Wiley; (I) Schematic illustration of the benefits of the layered-to-rocksalt atomic reconfiguration to the NFM/RS; (J) NFM and NFM/RS cathodes changed in lattice parameters *a*, *c* and *V*; (K) The thickness of CEI for NFM/RS after 200 cycles at 1 C. (I-K) are reprinted with permission from Ref.[51], Copyright © 2025 Elsevier. UHB: Upper hubbard band; LHB: lower hubbard band; TM-O: transition metal-oxygen; RS: rocksalt; NFM: $NaNi_{1/3}Fe_{1/3}Mn_{1/3}O_2$; CEI: cathode electrolyte interface; NFM/RS: $NaNi_{1/3}Fe_{1/3}Mn_{1/3}O_2$; LLO: Li-rich layered oxide; LZP: $LiZr_2(PO_4)_3$; XRD: X-ray diffraction.

SIBs are considered a promising alternative to LIBs due to their low cost and superior low-temperature performance[46]. However, most electrode materials exhibit sluggish kinetics and poor cycling stability. Layered transition metal oxides are particularly attractive cathode materials for SIBs due to their high energy density and elemental abundance[53]. Chen *et al.* designed a P2/Zig-Zag biphasic heterostructure cathode

featuring an atomic interlocking architecture[25] [Figure 3F]. This structure ensures continuous Na^+ migration pathways, while the "interlocking effect" suppresses interlayer gliding [Figure 3G], and the P2 phase reduces the Na^+ migration energy barrier. *In-situ* X-ray diffraction (XRD) results reveal that the volume expansion of the P2 phase within the biphasic heterostructure is effectively counterbalanced during charging, resulting in a smaller volume change as compared to the pure P2 phase [Figure 3H]. Owing to the low-resistance Na^+ migration pathways enabled by the heterostructures, the Na^+ diffusion coefficient increases to 10^{-9} cm^2 s^{-1} upon the P2/Zig-Zag to P2/P3 phase transition. For O3-type cathodes, the electrochemical performance is severely compromised when the pristine layered structure transforms into a cation-disordered rock-salt phase. To solve this issue, an O3-type $NaNi_{1/3}Fe_{1/3}Mn_{1/3}O_2$ (NFM/RS) layered-rock-salt heterostructure was developed based on an atomic reconstruction strategy[51] [Figure 3I], which exhibited superior hydrophobicity and imparted moisture resistance in air while simultaneously achieving typical quasi-zero-strain behavior with an overall volume change of only 0.72% [Figure 3J]. As a result, the NFM/RS cathode showed a thin and uniform cathode electrolyte interface (CEI) and maintained enhanced rate performance [Figure 3K].

Among anode materials for SIBs, transition metal sulfides (TMSs) offer high energy density due to their multi-electron transfer characteristics. However, the aggregation and deactivation of active particles remain major obstacles[57]. To address this, Zhang *et al.* designed an isotropic Co_9S_8/MoS_2 heterostructure to alleviate internal stress[54]. The preferential crystallographic orientation provides rapid Na^+ diffusion pathways, while the precisely synthesized isotropic heterostructures enable uniform Na^+ deposition [Figure 4A]. In this isotropic structure, Na^+ rapidly diffuses and distributes uniformly to the bottom, while the stress distribution remains dispersed, which avoids stress accumulation [Figure 4B]. Additionally, the abundant heterointerface effectively enhances electronic conductivity, synergistically improving reaction kinetics. In electrodes, vacancies not only increase reactive sites but also serve as bridges facilitating electron transfer between different semiconductors. The combination of heterostructures with vacancy engineering offers synergistic enhancements in both conductivity and kinetics. A ZnS-MoS_2 heterostructure with tunable S vacancy content can be prepared by temperature control to achieve superior sodium storage performance[55]. During heat treatment, the strong electronegativity of Mo favors bonding with S and generates the ZnS-containing S vacancies. Notably, the optimal vacancy signal was observed at 800 °C [Figure 4C]. Density functional theory (DFT) elucidates that the charge redistribution at the ZnS-MoS_2 interface effectively closes the bandgap, which yields the lowest Na^+ diffusion energy barrier of 0.15 eV [Figure 4D and E].

The potential of potassium (K^+/K: -2.93 V) is very close to that of lithium, which implies that the theoretical operating voltage of PIBs can be comparable to LIBs (approximately 3.5-4.0 V)[58]. According to the energy density formula $E = Q \times V$, the voltage advantage endows PIBs with the potential to surpass SIBs in terms of both power density and the upper limit of energy density[59]. Current research on PIBs focuses on addressing the severe volume expansion and sluggish diffusion kinetics arising from the large ionic radius of K^+[60]. In anode materials, constructing a heterointerface has proven to be an effective strategy to tackle these two core issues. Li *et al.* designed an N/$CoTe_2$ featuring self-catalytic N-Co bonds and a low-tortuosity 3D tunnel architecture for efficient potassium storage[61]. This heterostructure provides short-range and efficient electron/ion transport pathways. The *in-situ* formed N/Co@C self-catalytic centers significantly enhance the adsorption capability toward K_xTe_γ and accelerate their conversion kinetics.

The quantitative modulation of built-in electric fields within heterostructures represents a significant breakthrough in recent research. Song *et al.* achieved experimental quantification and tuning of the field intensity in FeSe/Fe_3Se_4[57] [Figure 4F]. By combining scanning Kelvin probe microscopy [Figure 4G], Zeta potential measurements, and transient photocurrent density analysis, they directly quantified the increase in intensity from 17.24 mV to 62.84 mV upon uniform Co doping [Figure 4H]. The enhanced electric fields

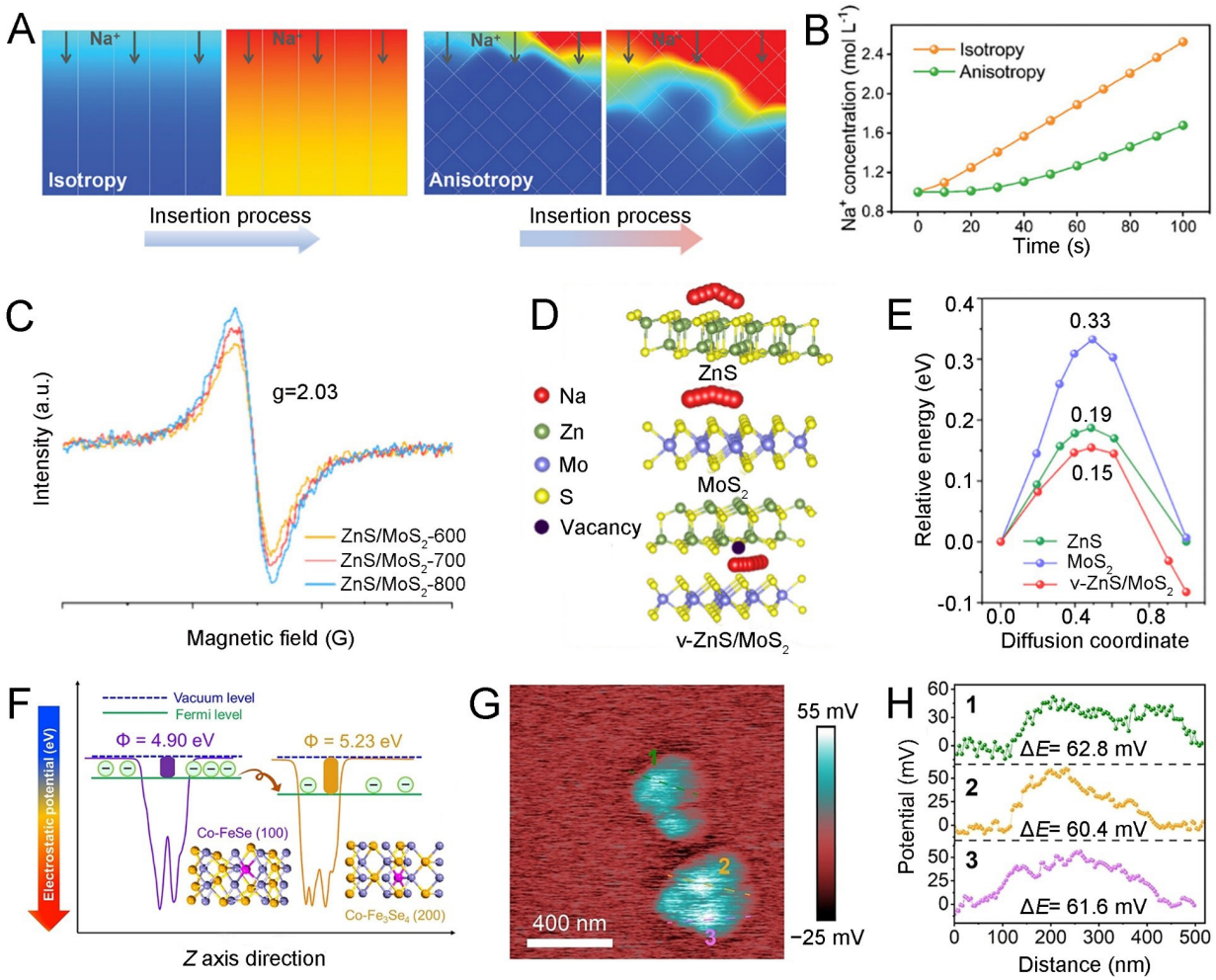

Figure 4. (A) Na^+ concentration distributions and (B) Na^+ concentration comparisons of the isotropic and anisotropic structure at the specific time in Co_9S_8/MoS_2 heterostructure. (A and B) are reprinted with permission from Ref.[54], Copyright © 2025 Wiley; (C) Electron paramagnetic resonance (EPR) spectra of ZnS/MoS_2-600, ZnS/MoS_2-700, and ZnS/MoS_2-800; (D) Na^+ migration paths and (E) diffusion energy barriers in ZnS/MoS_2. (C-E) are reprinted with permission from Ref.[55], Copyright © 2025 American Chemical Society; (F) Schematic diagram of work functions of Co/FeSe and Co/Fe_3Se_4 in Co/Fe_4Se_5 heterostructure; (G) SKPM image of Co/Fe_4Se_5@C heterostructure and (H) the concerned surface potential plots. (F-H) are reprinted with permission from Ref.[56], Copyright © 2024 Wiley. SKPM: Scanning kelvin probe force microscopy.

reduce the K^+ diffusion barrier from 0.53 eV to 0.34 eV and enable the electrode to maintain a high reversible capacity of 145.8 mAh g^{-1} at 10 A g^{-1}, with 95.1% capacity retention after 3000 cycles. Notably, this strategy demonstrates universality across heterostructures doped with other atoms (Cu/Ni), which provides a general approach for modulating interfacial electric field strength.

Lithium-sulfur batteries

LSBs are promising candidates for next-generation energy storage systems due to their high theoretical energy density (2,600 Wh kg^{-1}) as well as the resource abundance and environmental friendliness of sulfur[62,63]. However, the practical application of LSBs is hindered by three factors: the insulating nature of sulfur and its discharge products (Li_2S_2/Li_2S)[64], the shuttle effect and the sluggish reaction kinetics of LiPSs[65]. Heterostructure materials typically exhibit a synergistic "adsorption-catalysis" effect[66], which offers unique advantages in regulating LiPSs and accelerating redox kinetics. Although incorporating catalysts into the sulfur cathode can enhance the reaction kinetics, their adsorption-desorption kinetics toward LiPSs often remain unsatisfactory. To address this issue, Song *et al.* constructed a RuP_2-RuP heterostructure through a

temperature-controlled strategy[67] [Figure 5A], which exhibits excellent electronic conductivity, desirable adsorption capability for LiPSs, and high catalytic activity. DFT calculations reveal that the RuP_2-RuP exhibits the strongest adsorption affinity toward Li_2S_6, and the S-S bond length is elongated from 2.10-2.12 Å to 2.15 Å after adsorption, which facilitates the subsequent conversion of LiPSs [Figure 5B]. Moreover, the RuP_2-RuP heterostructure achieves a high Li_2S deposition capacity of 267 mAh g^{-1}, which further confirms its superior catalytic activity for the liquid-solid conversion. This work clearly demonstrates the critical role of interfacial coupling effects in heterostructures for simultaneously enhancing polysulfide anchoring and catalytic conversion. GeS_2/NiS_2 heterostructure can be designed as a catalytic sulfur host[68] [Figure 5C]. Metallic NiS_2 forms an ohmic contact with semiconducting GeS_2, which can create a highly conductive heterointerface [Figure 5D]. During reactions, NiS_2 acts as an emitter, rapidly injecting a large number of electrons into LiPSs through the GeS_2 base, thereby achieving a maximum reaction current amplification factor (β_R) of 105. Consequently, it can enhance the electron transfer kinetics [Figure 5E] and lead to a swift conversion of S_8 into LiPSs and uniform deposition of Li_2S on the surface of the $S@GeS_2/NiS_2$@rGO electrode.

Current interpretations of the role of sulfur hosts predominantly focus on the relationship between electronic energy levels and catalytic properties, while the contribution of electron spin is often overlooked. In fact, the spin-state configuration of transition metals is a key factor influencing the electronic structure of catalysts, which determines their orbital occupancy, activity, and selectivity[69]. Inspired by this, a hollow $NiS_2/NiSe_2$ heterostructure with a high-spin configuration was developed by Huang et al[70]. At the $NiS_2/NiSe_2$ heterointerface, the octahedral crystal field splitting energy of Ni^{3+} is modified, thus triggering electron transitions from the t_{2g} to e_g orbitals and inducing a low-spin to high-spin transition. In the high-spin state, the increased e_g electron occupancy upshifts the *d* band center, which strengthens orbital hybridization with the S 3*p* states of LiPSs. This heterostructure achieves significantly improved electrical conductivity and enhanced adsorption toward Li_2S_6. The nickel serves as the active site to supply abundant electrons to LiPSs to facilitate their reduction, which enables rapid reaction kinetics. The role of electron spin states is similarly evident in CoO/Mo_2C@CNFs (carbon nanofibers)[71] [Figure 5F]. In contrast to the high-spin state of nickel, the incorporation of molybdenum reduces the spin state of cobalt due to differences in crystal structure[72], and the resulting low-spin cobalt effectively mitigates the LiPSs shuttle effect through strong chemisorption of Co-S bonds. As a result, the CoO/Mo_2C@CNFs achieves a higher Li_2S precipitation capacity (165 mAh g^{-1}) than that of CoO@CNFs (60 mAh g^{-1}) and Mo_2C@CNFs (78 mAh g^{-1}) [Figure 5G].

For LSBs, the separator not only physically isolates the cathode and anode but also plays a critical role in regulating the LiPSs and Li^+ ion deposition behaviors[73-75]. A common strategy is the functional modification of the separator with a coating layer that imparts adsorption and catalytic capabilities. Heterostructured coating designs are particularly advantageous as they offer a catalytically active heterointerface while ensuring efficient Li^+ transport. Wu *et al.* designed a WB/WC heterostructure using an MBene material[74], where B forms strong coordination bonds (B-S) with the S atoms in LiPSs, which increases the density of catalytically active centers. *In-situ* Raman spectroscopy provides intuitive evidence that the WB/WC coating effectively blocks the LiPSs shuttle and promotes their reduction to Li_2S [Figure 5H]. Similarly, Ma *et al.* reported a MIL-88A/CdS heterostructure coating featuring nanoscale catalytic sites anchored on a micron-scale substrate[75] [Figure 6A], where the significant size disparity enhances the catalytic activity of CdS. MIL-88A/CdS shows a substantially lower diffusion energy barrier of Li_2S_6 (0.92 eV) than that on MIL-88A (1.80 eV) [Figure 6B], which indicates rapid migration to CdS catalytic sites. Time-of-flight secondary ion mass spectrometry (TOF-SIMS) reveals that LiPSs do not accumulate extensively on the surface but exhibit transient fluctuations followed by rapid stabilization [Figure 6C]. This observation reflects a strong interaction between the LiPSs and the heterostructure, which can significantly enhance sulfur utilization.

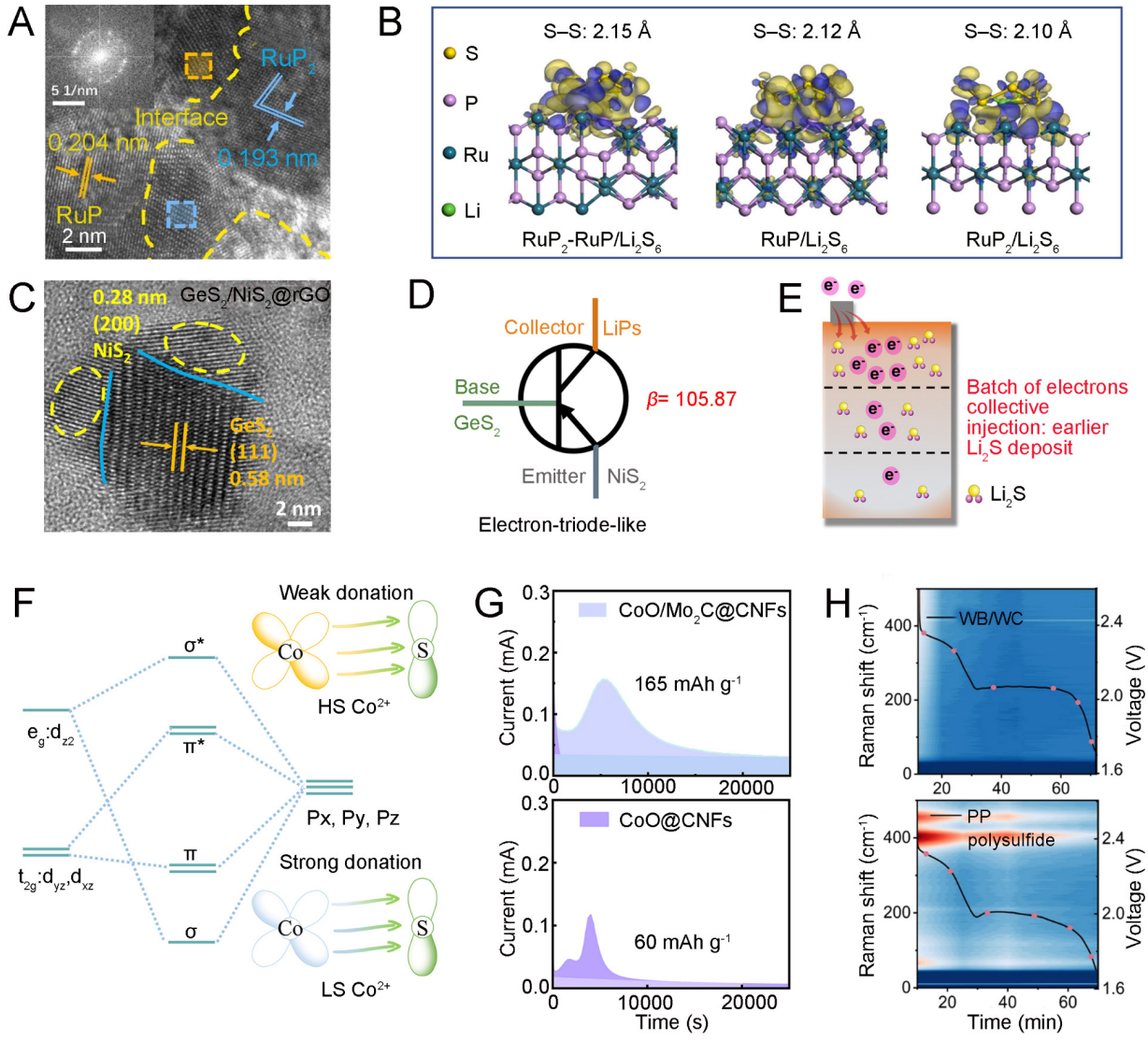

Figure 5. (A) HRTEM image of RuP_2/RuP heterostructure; (B) The simulated charge density difference isosurface of Li_2S_6 adsorbed on the surface of different catalysts. (A and B) are reprinted with permission from Ref.[67], Copyright © 2024 Elsevier; (C) HRTEM image of GeS_2/NiS_2@rGO; (D) Electron-triode-like GeS_2/NiS_2 heterostructure achieves 105.87 times current amplification; (E) Schematic diagram of the lithium-sulfur pouch battery, and the continuous reaction of transferred electrons results in an uneven electron distribution. (C-E) are reprinted with permission from Ref.[68], Copyright © 2025 Royal Society of Chemistry; (F) Scenario of *d-p* orbital hybridization and (G) current-time profile recorded under a constant potential of 2.05 V for charging in CoO/Mo_2C. (F and G) are reprinted from Ref.[71], under CC BY 4.0 license; (H) Corresponding planar time-resolved Raman spectra of pure PP and WB/WC-modified separator. (H) is reprinted from Ref.[74], under CC BY 4.0 license. rGO: Reduced graphene oxide; CNF: carbon nanofiber; HRTEM: high-resolutiontransmission electron microscope; LS: low spin; HS: high spin.

Beyond separator coating modifications, heterostructures employed as interlayers also effectively mitigate the shuttle effect and enhance the performance of LSBs. Xu *et al.* developed a ternary heterostructure of MoS_{2-x}/MoO_2/CoP with built-in electric fields and abundant S vacancies[78]. Each of the three components contributes distinct functionalities: MoS_{2-x} and CoP exhibit strong adsorption and catalytic capabilities, respectively, while MoO_2 possesses an intermediate work function that serves as a bridge between the electronic pathways [Figure 6D]. Adsorption experiments reveal that after interaction with Li_2S_6, the Mo 3*d* peaks of MoS_{2-}x/MoO_2/CoP shift toward lower binding energies, which highlights the strong interaction with Li_2S_6 [Figure 6E]. Moreover, MoS_{2-x}/MoO_2/CoP exhibits higher binding energies with LiPSs than other materials throughout six lithiation steps, implying outstanding adsorption performance. When employed as an interlayer in high-loading LSBs (7.13 mg cm^{-2}), the MoS_{2-}x/MoO_2/CoP delivers a stable capacity of 6.6

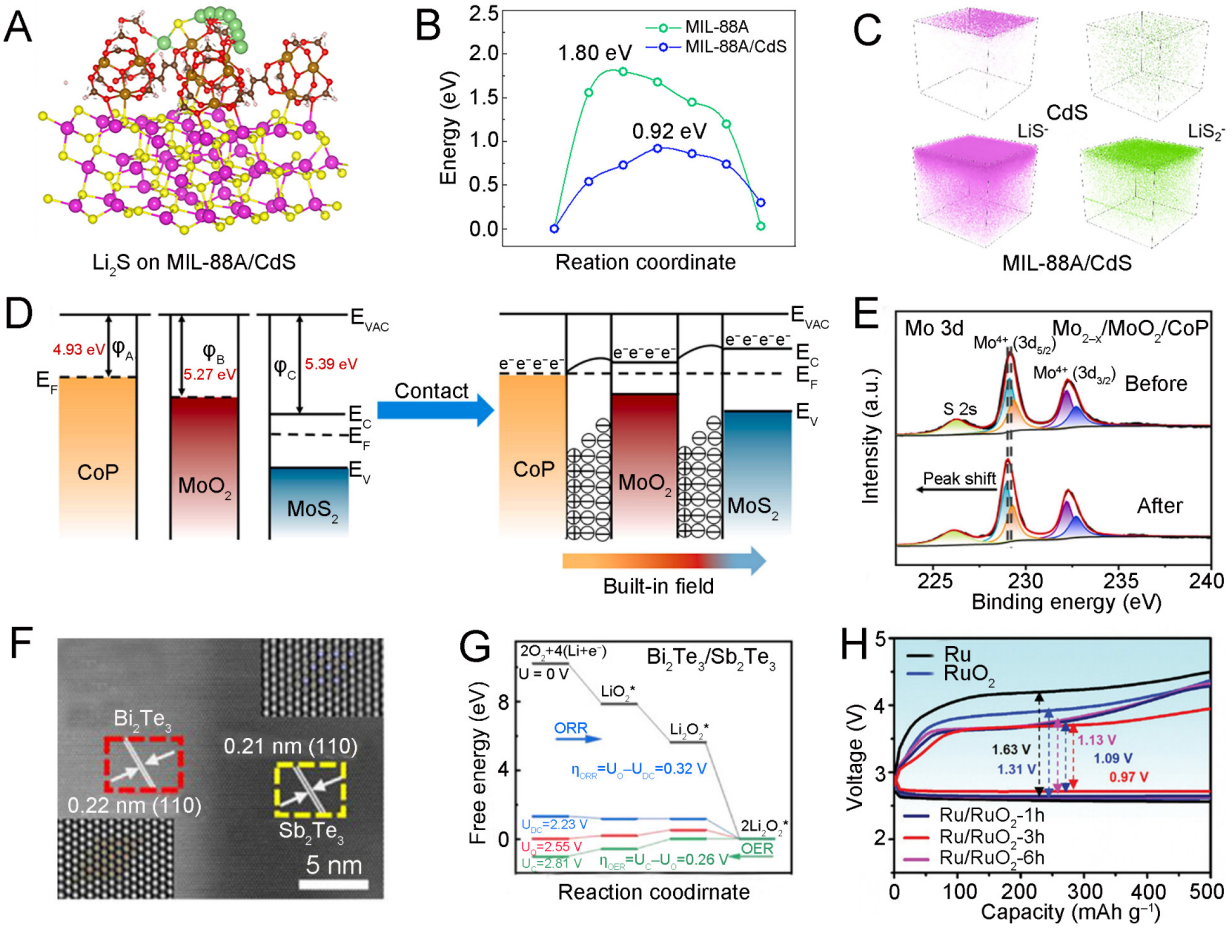

Figure 6. (A) Optimized configuration of Li_2S decomposition on MIL-88A/CdS; (B) Diffusion energy barrier of Li_2S_6 in MIL-88A/CdS; (C) TOF-SIMS 3D reconstructed images for LiS^- and LiS_2^- secondary ions of CdS and MIL-88A/CdS. (A-C) are reprinted from Ref.[75], under CC BY 4.0 license; (D) Energy-band diagrams of MoS_{2-x}/MoO_2/CoP ternary heterostructure before and after contact formation of the built-in electric fields; (E) Mo 3*d* spectra of MoS_{2-x}/MoO_2/CoP before and after adsorbing Li_2S_6. (D and E) are reprinted with permission from Ref.[78], Copyright © 2025 Elsevier; (F) TEM image of Bi_2Te_3/Sb_2Te_3. Figure F is reprinted with permission from Ref.[79], Copyright © 2025 Wiley; (G) Energy diagrams of Bi_2Te_3/Sb_2Te_3; (H) Discharge/charge curves with current density 500 mA g^{-1} of Ru/RuO_2 cathodes. (G and H) are reprinted with permission from Ref.[80], Copyright © 2025 Wiley. TOF-SIMS: Time-of-flight secondary ion mass spectrometry; TEM: transmission electron microscope.

mAh cm^{-2} after 100 cycles.

Metal-air batteries

Metal-air batteries achieve energy conversion through the oxygen reduction reaction (ORR) at the cathode and the metal oxidation reaction at the anode, which has two fundamental advantages[81]. Firstly, they theoretically deliver exceptionally high energy densities (e.g., Li-O_2 > 3,500 Wh kg^{-1}). Secondly, the O_2 is sourced directly from the environment without the need for harsh reaction conditions, which can fundamentally reduce material and construction costs. On the cathode, both the ORR and the OER suffer from intrinsically sluggish kinetics, which necessitates efficient catalysts to lower the overpotentials. One critical advance is the design of coherent heterostructures with minimal lattice mismatch, which enables strong interfacial interactions and enhanced structural stability. Feng *et al.* developed a 2D Bi_2Te_3/Sb_2Te_3 heterostructure with exposed (001) facets as a catalyst for Li-O_2 batteries[79] [Figure 6F]. Owing to the low lattice mismatch (< 3%) between Bi_2Te_3 and Sb_2Te_3, the coherent interface ensures seamless atomic arrangement and minimizes stress accumulation. The built-in electric fields modulate the asymmetric charge distribution of Te atoms and enhance the adsorption of intermediate LiO_2, which facilitates charge transfer

between the adsorbed species and the catalyst [Figure 6G]. Consequently, the Bi_2Te_3/Sb_2Te_3 cathode delivers remarkable cycling stability in both pure oxygen and ambient air.

Compared to coherent heterostructures, Mott-Schottky heterostructures offer useful platform for accelerating ORR/OER kinetics by leveraging the spontaneous electron transfer at metal-semiconductor interfaces. Sun *et al.* constructed a Ru/RuO_2 heterostructure by partial oxidation[80]. The Ru/RuO_2 heterointerface modulates the *d*-band center to an optimal position, which balances the adsorption energies of oxygen-containing intermediates. The moderate binding strength for LiO_2 and Li_2O_2 enables efficient conversion along a two-electron pathway with minimal overpotential [Figure 6H]. Beyond metal oxide systems, multi-component Mott-Schottky heterostructures have also demonstrated remarkable catalytic capabilities. Xia *et al.* designed a self-supported $NiCo_2O_4/MnO_2$ heterostructure with vertically aligned nanosheet arrays on Ti paper[82] [Figure 7A]. The Mott-Schottky heterointerface weakens the adsorption of the LiO_2 intermediate to an optimal level, which can promote the formation of chip-like Li_2O_2 intimately embedded within the nanosheet arrays. Besides, the unique morphology provides abundant contact sites for catalysts and achieves efficient decomposition during charging [Figure 7B]. These merits enable the $NiCo_2O_4/MnO_2$-based electrode to achieve 800 cycles and a remarkably low overpotential of 0.73 V that outperforms the $NiCo_2O_4$.

Zinc-air batteries (ZABs) possess high theoretical energy density and inherent safety. However, the reactions involve multi-step electron transfer processes and high overpotentials[88]. An essential approach to achieve exceptional bifunctional activity is the precise engineering of atomic-scale heterostructures that combine dual-atom sites with adjacent nanoclusters. Lu *et al.* developed a porous carbon fiber membrane decorated with atomically dispersed CoN_4/FeN_4 dual sites and neighboring Co_2Fe_2/Fe_5 nanoclusters[83]. The Fe_5 cluster significantly weakens the Fe-OH coupling at the FeN_4 site, which lowers the energy barrier for the rate-determining step of ORR from 0.59 eV to 0.46 eV, while the Co_2Fe_2 cluster enhances Co-OH interaction to promote OER kinetics [Figure 7C]. This synergistic effect endows the catalyst with outstanding ORR (0.87 V) and OER (1.58 V) performance. Zhang *et al.* constructed a Janus $CeO_2/ZnCoS$ heterostructure[84] [Figure 7D], in which the intimate heterointerface induces strong electronic coupling, thus generating abundant O and S vacancies that serve as additional active sites. The $CeO_2/ZnCoS$ with S vacancies exhibits up-shifted *d*-band centers and optimized adsorption energies for intermediates, resulting in a reduced overpotential for the rate-determining step of ORR (0.32 V) as compared to single-phase ZnCoS (0.82 V). When integrated into ZABs, it delivers a peak power density of 168.7 mW cm^{-2} [Figure 7E], and exhibits enhanced cycling stability over 865 cycles.

Another way to enhance air cathode performance is the design of self-reconstructed heterostructures. A Co/Co2P heterostructure can be embedded in P/N-codoped carbon nanofibers (Co/Co2P@PNCF) as a cathode for Zn-Co/air hybrid batteries [85]. During the first cycle, the Co/Co_2P undergoes deep self-reconstruction and generates high-valent Co species (Co^{3+}/Co^{4+}) that serve as highly active redox centers. The reversible transformation between $Co^{3+/4+}O_x(OH)_y$ and $K_xCo^{2+/3+}O_y$ during cycling enhances OER activity and provides additional charging-discharging plateaus, which promotes the Zn-Co/air hybrid batteries to deliver high power density and cycling stability [Figure 7F and G]. A key kinetic bottleneck in ORR that has been largely overlooked is the acceleration of the proton-coupled electron transfer. Zhang *et al.* developed an $Fe_2N/CrNx$ heterostructure catalyst supported on N-doped carbon (Fe_2N/CrN_x@NC) for aluminum-air batteries (AABs)[87]. In this heterostructure, Fe_2N serves as the primary ORR active sites, while CrN_x clusters enhance H_2O dissociation kinetics, which acts as a continuous proton supply to accelerate the protonation of intermediates[89]. Meanwhile, the Fe_2N/CrN_x heterointerface induces strong *d-d* orbital hybridization, which upshifts the *d*-band center of Fe atoms, thereby optimizing the adsorption energy of ORR intermediates. The synergistic effect reduces the overpotential from 0.68 V (Fe_2N@NC) to 0.55 V (Fe_2N/CrN_x@NC). Using a

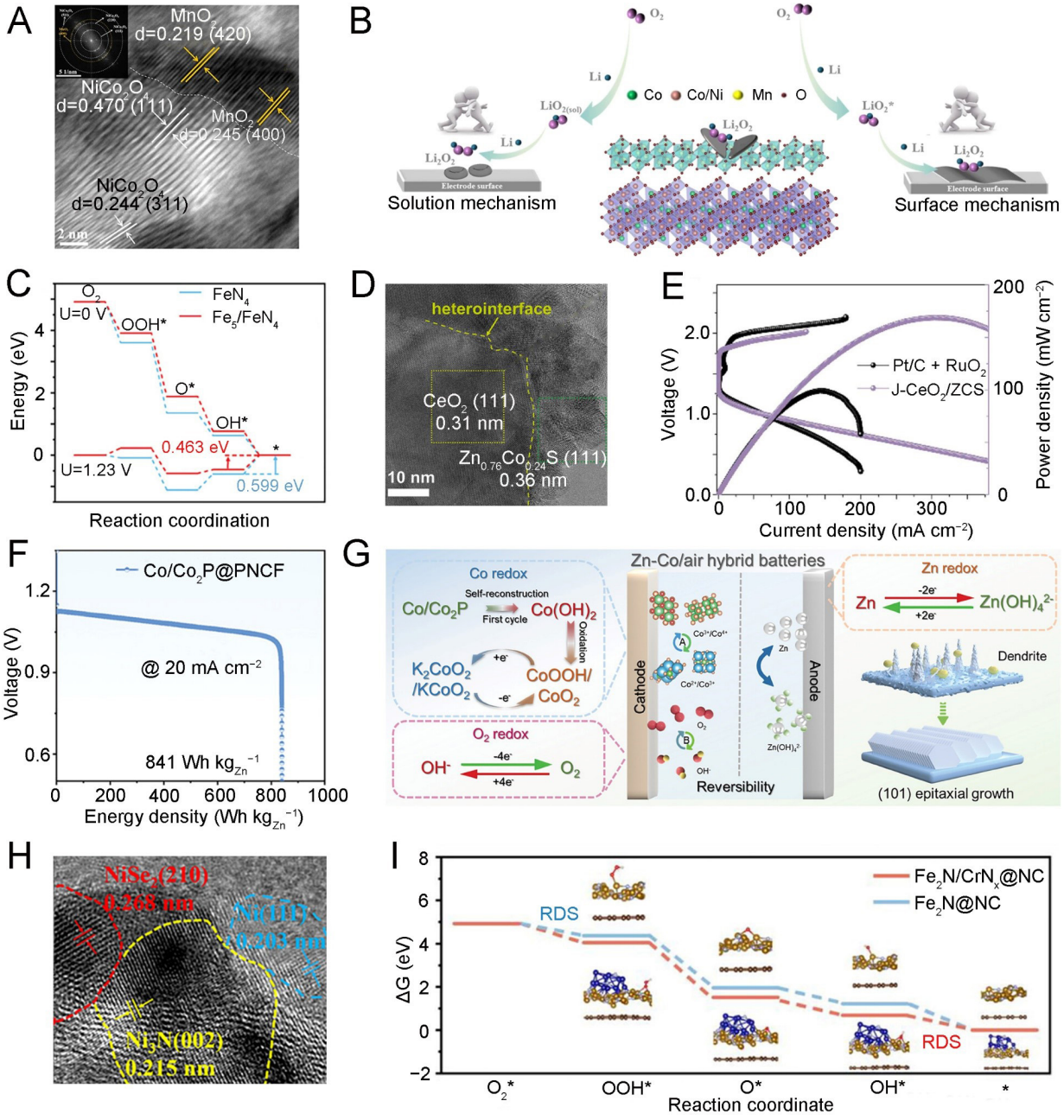

Figure 7. (A) HRTEM image and (B) schematic reaction mechanism of $NiCo_2O_4/MnO_2$. (A and B) are reprinted from Ref.[82], under CC BY 4.0 license; (C) ORR free energy diagrams for FeN_4 and Fe_5/FeN_4 sites at 0 and 1.23 V *vs.* RHE. (C) is reprinted with permission from Ref.[83], Copyright © 2025 Wiley; (D) HRTEM image of CeO_2/ZnCoS; (E) Charge/discharge polarization and corresponding power density curves of ZABs employing CeO_2/ZnCoS and Pt/C + RuO_2 as air cathodes. (D and E) are reprinted with permission from Ref.[84], Copyright © 2024 Elsevier; (F) Energy density curve of Co/Co_2P at 20 mA cm^{-2}; (G) Reaction mechanism of Zn-Co/air hybrid batteries. (F and G) are reprinted with permission from Ref.[85], Copyright © 2025 Wiley; (H) TEM image of p-$NiSe_2$/Ni/Ni_3N@NCNT@CC. (H) is reprinted with permission from Ref.[86], Copyright © 2025 Wiley; (I) Gibbs free energy diagrams of ORR for Fe_2N@NC and Fe_2N/CrNx@NC at U = 0 V. (I) is reprinted with permission from Ref.[87], Copyright © 2026 Wiley. PNCF: P/N-codoped carbon nanofiber; NC: N-doped carbon; HRTEM: high-resolution transmission electron microscope; TEM: transmission electron microscope; RHE: ORR: oxygen reduction reaction.

plasma-assisted nitridation strategy, Xu *et al.* designed a Se vacancy-rich ternary heterostructure of $NiSe_2$/Ni@Ni_3N catalyst[86] [Figure 7H]. The plasma treatment can introduce abundant Se vacancies and carbon defects. This unique ternary architecture combines the metallic conductivity of Ni, the catalytic activity of $NiSe_2$, and the structural stability of Ni_3N, while Se vacancies modulate the electronic structure of the active Ni sites[87]. This enables the AABs to exhibit a small bifunctional potential gap (ΔE = 0.74 V) and

deliver a peak power density of 106.8 mW cm^{-2} with stable cycling over 1,000 cycles [Figure 7I].

Aqueous batteries

Aqueous batteries have attracted considerable attention owing to their intrinsic safety, environmental friendliness, and cost-effectiveness[90,91]. However, their development has been persistently hindered by low energy density and insufficient stability. The narrow thermodynamic stability window of water molecules (~ 1.23 V) makes the hydrogen evolution reaction (HER) a critical bottleneck limiting Coulombic efficiency and cycle life. Concurrently, metal anodes are prone to corrosion and dendrite growth in an aqueous environment. In addition, the aqueous environment readily induces dissolution and structural collapse of active materials, and most cathode materials exhibit insufficient intrinsic electronic conductivity, resulting in poor rate capability. These interconnected issues collectively constitute the core obstacles hindering the practical application of aqueous batteries.

Heterostructure strategies offer a promising way to overcome these barriers. For instance, MnO_2 is widely utilized in aqueous zinc-ion batteries (ZIBs) due to its high theoretical capacity of 308 mAh g^{-1} and a suitable voltage window (1.3-1.4 V *vs.* Zn^{2+}/Zn)[92]. Nevertheless, Mn^{3+} is prone to both disproportionation reactions ($2Mn^{3+} \rightarrow Mn^{2+} + Mn^{4+}$) and Jahn-Teller distortion, which exacerbate manganese dissolution and structural instability. Therefore, constructing heterostructures to enhance the electrochemical activity of Mn-based materials is an effective strategy for improving stability. Based on this, Zhao *et al.* proposed a dynamic transformation strategy that effectively reduces the formation of the irreversible byproduct $ZnMn_2O_4$, which suppresses Mn dissolution and enhances electronic conductivity[93]. The prepared $Bi_{12.53}Mn_{0.47}O_{19.85}$/R-$MnO_2$ (BiO/MnO_2) heterostructure features BiO acting as a reservoir for Bi^{3+} [Figure 8A]. During reaction, BiO can directly supply Bi^{3+} to R-MnO_2, leading to the *in-situ* formation of $Bi_2Mn_4O_{10}$ (BMO) [Figure 8B], which facilitates a dynamic transformation from BiO/MnO_2 to BMO/MnO_2. During this process, the concentration of dissolved Bi^{3+} in the electrolyte tends to stabilize, and the dynamic transformation gradually reaches equilibrium, which creates a more abundant heterointerface, avoids spontaneous dissolution of Mn, and enhances reaction kinetics. Consequently, the BiO/MnO_2 based aqueous ZIB exhibits a high rate capability (204.5 mA h g^{-1} at 4 A g^{-1}) and superior cycling stability (no capacity decay after 2,000 cycles at 2 A g^{-1}).

During the zinc deposition process, the hydrated zinc ion $[Zn(H_2O)_6]^{2+}$ first overcomes a substantial desolvation energy barrier to strip off its coordinated water molecules, which allows the bare Zn^{2+} to gain electrons and plate onto the anode surface[94]. Sluggish desolvation kinetics cause the accumulation of Zn^{2+} at the interface, which can induce uneven Zn deposition. Moreover, the intercalation of large-radius hydrated Zn^{2+} causes irreversible structural evolution of the electrode and results in diminished cycling stability. Consequently, the desolvation step constitutes a critical bottleneck for interfacial reaction kinetics. To address this, a TiS_2/TiO_2 heterostructure was designed to simultaneously promote interfacial desolvation and ion/electron transfer[95] [Figure 8C]. The built-in electric fields in TiS_2/TiO_2 provide a separating force for charged Zn^{2+} and electrically neutral water molecules, which effectively reduces the desolvation barrier [Figure 8D] and promotes the transformation of $[Zn(H_2O)_6]^{2+}$ into Zn^{2+} during the desolvation process. The resultant mitigation of lattice distortion contributes to an extended cycle life. Furthermore, the synergistic effect of the built-in electric fields and vacancies accelerates Zn^{2+} diffusion within the bulk structure. This contributes to a high reversible capacity of 160.9 mAh g^{-1} even at a high current density of 5 A g^{-1}. Moreover, Wang *et al.* subsequently designed a zinc hydroxide chloride (ZHC) and Cu heterostructure, which effectively guides efficient Zn deposition [Figure 8E][94]. ZHC with hydrophilic/zinophobic properties can facilitate the desolvation of hydrated Zn^{2+} prior to Zn nucleation, while the adjacent Cu serves as a zincophilic site for subsequent nucleation and deposition. This accelerates Zn^{2+} deposition kinetics and effectively suppresses the hydrogen evolution side reactions.

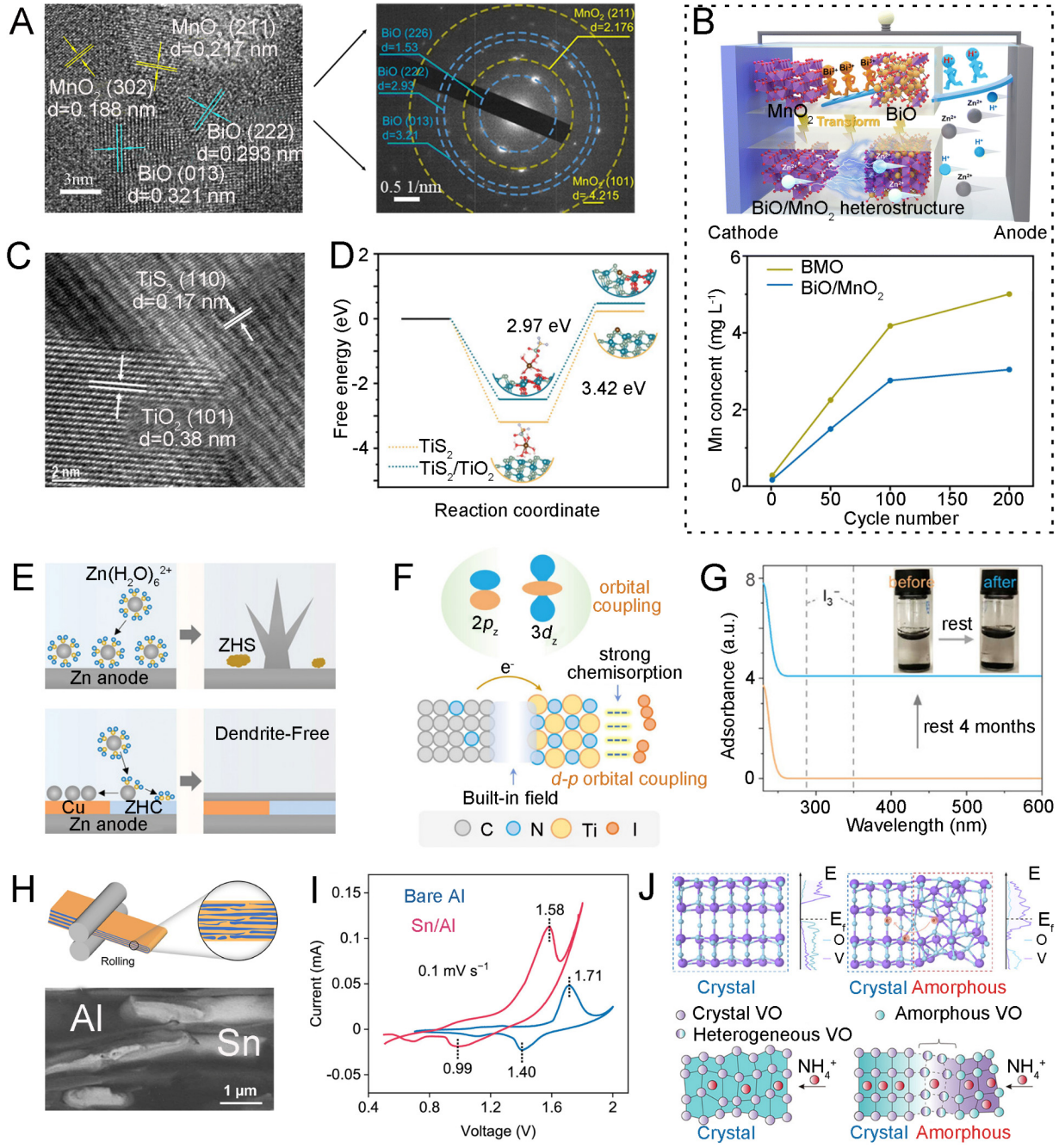

Figure 8. (A) HRTEM image of BiO/MnO_2 with SAED pattern; (B) Schematic of Zn||BiO/MnO_2 battery. (A and B) are reprinted with permission from Ref.[93], Copyright © 2024 Royal Society of Chemistry; (C) HRTEM of TiS_2/TiO_2 heterostructure; (D) Energy barriers for the desolvation process of the $[Zn(H_2O)_5]^{2+}(CF_3SO_3)^-$ solvated structure on different crystal structures. (C and D) are reprinted with permission from Ref.[95], Copyright © 2025 Wiley; (E) Schematic illustrations of Zn deposition at different interfaces of bare Zn and ZHC/Cu@Zn. (E) is reprinted with permission from Ref.[94], Copyright © 2024 Wiley; (F) Schematic illustration of interfacial electronic interaction in PNC/TiN; (G) UV-vis absorbance spectra of PNC/TiN-I_2 before and after being immersed in electrolyte for 4 months. (F and G) are reprinted with permission from Ref.[96], Copyright © 2026 Wiley; (H) Characterization of Sn/Al; (I) CV curves of Al||Al_xMnO_2 and Sn/Al||Al_xMnO_2 cells at a scan rate of 0.1 mV s^{-1}. (H and I) are reprinted with permission from Ref.[97], Copyright © 2024 Elsevier; (J) Illustration of the improvement in conductivity and NH_4^+ conduction in crystalline-amorphous VO heterostructure.(J) is reprinted with permission from Ref.[98], Copyright © 2025 American Chemical Society. ZHS: Zinc hydroxysulfate; ZHC: zinc hydroxide chloride; HRTEM: High-resolution transmission electron microscope; SAED: selected area electron diffraction; CV: cyclic voltammetry; PNC: porous N-doped carbon.

Heterostructure materials capable of suppressing the shuttle effect are also applicable to aqueous zinc-iodine batteries. A biomass-derived porous N-doped carbon (PNC) coated with TiN (PNC/TiN) has recently been reported as an advanced iodine host[96]. During the reaction, the upshift of the Ti *d*-band center enables

orbital coupling between the Ti 3*d* and I 5*p* states, which enhances the affinity for iodine while suppressing polyiodide shuttling [Figure 8F]. UV-vis spectroscopy reveals that no iodine absorption peaks are detected in the PNC/TiN-I_2 solution even after four months of rest, which corroborates the exceptional chemical immobilization of iodine species within the host structure [Figure 8G]. This design ultimately achieves an average Coulombic efficiency of 99.93% over 66,000 cycles.

Aqueous aluminum-metal batteries offer high theoretical energy density because Al^{3+} transfers three electrons during redox reactions[99]. Nevertheless, they face critical challenges, including poor reversibility of Al deposition, the formation of a passive layer, and the competing HER. A proven strategy involves introducing foreign metals to interact with Al. The Sn/Al heterostructure using Sn with a higher work function (4.42 eV) than Al (4.28 eV) can guide the underpotential deposition (UPD) of Al^{3+}[97]. The UPD process, in which metal deposition occurs on a substrate at a potential less negative than its thermodynamic deposition potential, realizes efficient and controlled Al deposition. This Sn/Al heterostructure effectively promotes Al stripping/plating and reduces internal resistance. Remarkably, the surface oxide layer on Sn/Al is prone to fracture and fragmentation during rolling, resulting in a uniform distribution of the oxide throughout the composite structure without completely covering the composite surface [Figure 8H]. These results confirm that the Sn framework not only helps maintain structural stability but also generates SnO_2 during cycling, which introduces higher electronic conductivity and enhances ion diffusion. As a result, the Sn/Al||Sn/Al symmetric cells exhibit stable cycling for over 900 hours with a low overpotential < 0.5 V. In full cells, the Sn/Al (1.40 V) anode shows a higher reduction peak than that observed for bare Al (0.99 V), and the energy density is improved [Figure 8I].

Aqueous ammonium-ion batteries leverage the adsorption characteristics of non-metallic charge carriers to achieve superior volumetric energy density and rate capability[100]. V-based materials have been widely adopted due to their excellent structural integrity and ability to accommodate the large ionic radius of NH_4^+. Yang *et al.* developed a crystalline-amorphous VO_2 heterostructure (SR-VO) via controlled $NaBH_4$ etching of VO_2 nanobelts[98]. The heterointerface formed between metallic amorphous VO_x and semiconducting crystalline VO_2 substantially improves electronic conductivity and reduces the NH_4^+ adsorption energy to -2.20 eV, thereby accelerating charge transfer and ion diffusion [Figure 8J]. Critically, the amorphous layer acts as a dynamic lattice-self-adaptation buffer that can relieve intercalation-induced mechanical stress, in stark contrast to the severe lattice expansion observed in pristine VO_2. The synergistic effect of the built-in electric fields and the mechanical buffering of the amorphous layer endows SR-VO with exceptional cycling stability, which delivers a capacity of 83.4 mAh g^{-1} after 10,000 cycles at 10 A g^{-1} with a decay rate of only 0.004% per cycle. This strategy has also been demonstrated to be universally applicable to other V-based materials (e.g., $NH_4V_6O_{10}$, V_6O_{13}, V_2O_5).

CONCLUSION AND OUTLOOK

This review emphasizes the heterointerface with clear structures and charge reconfiguration effects. In applications, heterostructures effectively buffer volume expansion, induce uniform alkali-metal plating, and inhibit dendrite growth at the anode. The adsorption-catalysis tandem mechanism can effectively promote the conversion efficiency of key intermediates such as LiPSs and Li_2O_2 at the cathode. The incorporation of artificial heterostructure interlayers provides critical support for constructing stable batteries capable of operating at high voltage or over a wide temperature range. Notably, the advantages of heterostructure engineering are not confined to a single electrochemical system; they demonstrate cross-system adaptability, establishing a methodological foundation for the design of universal high-performance electrodes. Nevertheless, practical applications remain an ongoing challenge, and further efforts are still needed to address this issue:

1) Artificial intelligence (AI) assistance and big-data screening. Constructing large-scale databases of properties and integrating machine learning models such as graph neural networks (GNNs) or random forests, AI enables rapid and low-cost prediction of key parameters. These labels are derived from DFT calculations or literature mining, which allows efficient screening of high-potential heterostructures from a vast number of candidate combinations and significantly narrows the scope of experimental verification.

2) Deep mechanistic understanding of heterointerface. Advanced *in situ* characterization techniques and DFT calculations can be utilized to reveal the dynamic evolution mechanisms of the heterointerface, including phase transitions, defect generation, interface reconstruction, and charge redistribution. These methods capture transient interfacial behaviors and elucidate the fundamental principles governing redox reactions and synergistic effects among components. These provide both theoretical guidance for the rational design and performance optimization of heterostructures.

3) Controlled synthesis and scalable fabrication. More efforts should be focused on developing controllable synthesis strategies for heterostructures. Currently, most heterostructures still rely on complex, low-yield synthetic routes, while two core issues remain to be solved: (1) achieving atomic-scale uniformity at the heterointerface; (2) poor batch-to-batch reproducibility due to the high sensitivity of reaction kinetics to parameters such as temperature gradients and precursor concentration fluctuations. Synergistic techniques such as vapor deposition, template epitaxy, and interfacial self-assembly should be explored to promote engineering applications. Based on these, two feasible technical routes are proposed: (1) Atomic layer deposition or molecular beam epitaxy can be employed in a model interface. (2) Microwave-assisted synthesis or continuous-flow microreactors are recommended when combined with *in situ* monitoring to realize closed-loop feedback control in reproducible large-scale applications.

4) Cross-component compatibility and commercialization pathways. In the future, the interfacial compatibility and overall matching degree between heterostructures and other components (such as electrolytes, binders and conductive agents) are critical. Such characteristics must be verified in industrial-scale devices. A comprehensive evaluation system can lay the foundation for the commercial application of heterostructures.

In summary, the research on heterostructures for electrochemical energy storage is entering a critical transition period from structural innovation to engineering scale-up. Only by achieving systematic breakthroughs in core areas such as quantitative mechanisms, controllable preparation, and full-cell compatibility can heterostructures advance more rapidly toward industrial applications. These provide a solid foundation for next-generation high-safety energy storage technology.

DECLARATIONS

Authors' contributions

Writing-original draft: Yang, Z.; Yuan, W.
Writing-review & editing: Ozoemena, K. I.; Eliseeva, S.; Wang, T.; Wu, Y.
Collecting & analyzing: Wang, T.
Supervision: Wang, T.; Wu, Y.
Funding acquisition: Wang, T.; Wu, Y.

Availability of data and materials

Not applicable.

AI and AI-assisted tools Statement

Not applicable.

Financial support and sponsorship

This work was supported by the National Natural Science Foundation of China (22279016), Zhishan Young Scholar Program of Southeast University (2242024RCB0004), and Start-up Research Fund of Southeast University (RF1028623005). Y.W. acknowledges the support by the Project on Carbon Emission Peak and Neutrality of Jiangsu Province (BE2022031-4), National Natural Science Foundation of China (52131306 and 52073143), the National Key Research and Development Program of China (2021YFB2400400), and Fundamental Research Funds for the Central Universities (2242023R10001).

Conflicts of interest

Wu, Y. is the Editor-in-Chief, and Ozoemena, K. I. is an International Advisory Editorial Board Member of the journal *Energy Z*, but were not involved in any steps of editorial processing, notably including reviewer selection, manuscript handling, and decision making, while the other authors have declared that they have no conflicts of interest.

Ethical approval and consent to participate

Not applicable.

Consent for publication

Not applicable.

Copyright

REFERENCES

1. Khan, M. A.; Thatipamula, S.; Tresca, L.; Xu, L.; Trewartha, A.; Onori, S. High-power lithium-ion battery characterization dataset for stochastic battery modeling. *Sci. Data.* **2025**, *12*, 1506. DOI PubMed PMC
2. Park, G.; Park, N.; Ryu, J.; et al. Zero-strain Mn-rich layered cathode for sustainable and high-energy next-generation batteries. *Nat. Energy.* **2025**, *10*, 1215-25. DOI
3. Chacana-olivares, J.; Peceño, B.; Grageda, M.; Cruz, C.; Rojas, L. Lithium-ion battery recycling: a perspective on key challenges and opportunities. *npj. Mater. Sustain.* **2025**, *3*, 38. DOI
4. Hu, J.; Fu, P.; Wei, Z.; et al. Early prediction of lithium-ion battery degradation with a generative pre-trained transformer. *Nat. Commun.* **2025**, *17*, 126. DOI PubMed PMC
5. Chen, S.; Dai, F.; Cai, M. Opportunities and challenges of high-energy lithium metal batteries for electric vehicle applications. *ACS. Energy. Lett.* **2020**, *5*, 3140-51. DOI
6. Xu, J.; Cai, X.; Cai, S.; et al. High-energy lithium-ion batteries: recent progress and a promising future in applications. *Energy. Environ. Mater.* **2023**, *6*, e12450. DOI
7. Li, Y.; Zhang, J.; Chen, Q.; Xia, X.; Chen, M. Emerging of heterostructure materials in energy storage: a review. *Adv. Mater.* **2021**, *33*, 2100855. DOI
8. Wang, S.; Zhao, S.; Guo, X.; Wang, G. 2D material-based heterostructures for rechargeable batteries. *Adv. Energy. Mater.* **2021**, *12*, 2100864. DOI
9. Huang, S.; Wang, Z.; Von Lim, Y.; et al. Recent advances in heterostructure engineering for lithium-sulfur batteries. *Adv. Energy. Mater.* **2021**, *11*, 2003689. DOI
10. Zhao, X.; Liu, M.; Wang, Y.; et al. Designing a built-in electric field for efficient energy electrocatalysis. *ACS. Nano.* **2022**, *16*, 19959-79. DOI
11. Li, Y.; Wu, F.; Qian, J.; et al. Metal chalcogenides with heterostructures for high-performance rechargeable batteries. *Small. Sci.* **2021**, *1*, 2100012. DOI
12. Gabriel, E.; Ma, C.; Graff, K.; Conrado, A.; Hou, D.; Xiong, H. Heterostructure engineering in electrode materials for sodium-ion batteries: recent progress and perspectives. *eScience* **2023**, *3*, 100139. DOI
13. Mei, J.; Liao, T.; Sun, Z. 2D/2D heterostructures: rational design for advanced batteries and electrocatalysis. *Energy. Environ. Mater.* **2021**, *5*, 115-32. DOI
14. Chen, L.; Ren, J. T.; Yuan, Z. Y. Enabling internal electric fields to enhance energy and environmental catalysis. *Adv. Energy. Mater.* **2023**, *13*, 2203720. DOI
15. Fu, H.; Wen, Q.; Li, P. Y.; et al. Recent advances on heterojunction-type anode materials for lithium-/sodium-ion batteries. *Small. Methods.* **2022**, *6*, 2201025. DOI

16. Zhou, W.; Lin, J.; Tang, Y.; et al. Catalyst for polysulfide conversion by Mo_2C/MoO_3 hybrids modified separator in lithium-sulfur batteries. *Mater. Today. Phys.* **2023**, *37*, 101193. DOI
17. Oh, H. G.; Jang, S.; Kim, H. R.; et al. Interface-engineered 3D ZnTe/MXene heterostructures with built-in electric fields for fast and durable potassium storage. *J. Energy. Chem.* **2025**, *111*, 462-73. DOI
18. Xie, J.; Li, Z.; Zheng, X.; Tian, F.; Lei, D.; Wang, C. Built-in electric field of *in situ* formed artificial interface layer induces fast and uniform sodium-ions transmission to achieve a long-term stable sodium metal battery under harsh conditions. *Adv. Funct. Mater.* **2024**, *34*, 2315309. DOI
19. Cai, W.; Zhang, X.; Hu, J.; et al. Electrochemically activated α → β phase transition in space-confined MnO/MnSe-based heterostructure enabling exceptional Li/Na-ion storage. *Small* **2026**, *22*, e00045. DOI
20. Cui, W.; Wang, P.; Li, X.; et al. Rich lattice defects Ni-MoO_2/$NiMoO_4$- bifunctional catalyst for efficient and stable seawater electrolysis hydrogen production. *J. Mater. Sci. Technol.* **2025**, *235*, 222-31. DOI
21. Sun, S.; Han, Z.; Liu, W.; et al. Lattice pinning in MoO_3 via coherent interface with stabilized Li^+ intercalation. *Nat. Commun.* **2023**, *14*, 6662. DOI
22. Liu, F.; Sun, X.; Liu, Y.; Song, X.; Gao, J.; Qin, G. TiO_2 nanorods confined in porous V_2O_5 nanobelts and interconnected carbon channels for sodium ion batteries. *Appl. Surf. Sci.* **2019**, *473*, 873-84. DOI
23. Le, T.; Yang, C.; Lv, W.; et al. Deeply cyclable and ultrahigh-rate lithium metal anodes enabled by coaxial nanochamber heterojunction on carbon nanofibers. *Adv. Sci.* **2021**, *8*, 2101940. DOI
24. Xiong, P.; Zhang, F.; Zhang, X.; et al. Strain engineering of two-dimensional multilayered heterostructures for beyond-lithium-based rechargeable batteries. *Nat. Commun.* **2020**, *11*, 3297. DOI PubMed PMC
25. Chen, Y.; Fan, Q.; Wang, H.; et al. Heterostructured manganese-based cathode with atomic interlocking for advanced sodium-ion batteries. *Adv. Energy. Mater.* **2025**, e04637. DOI
26. Yang, M.; Lin, Y.; Chen, P.; et al. Unlocking ultrafast-kinetics asymmetric heterojunction with multi-anionic redox chemistry enables high energy/power density and low-temperature zinc-ion batteries. *Angew. Chem. Int. Ed.* **2025**, *64*, e202510907. DOI
27. Gong, F.; Chen, Z.; Chang, C.; et al. Hollow Mo/MoS_{Vn} nanoreactors with tunable built-in electric fields for sustainable hydrogen production. *Adv. Mater.* **2024**, *37*, 2415269. DOI
28. Jia, X.; Zhao, Y.; Bai, L. First-principles investigation of interfacial interactions of BP/$Ti_3C_2S_2$ heterostructure regulating the anchoring performance in lithiumsulfur batteries. *J. Energy. Storage.* **2025**, *132*, 117859. DOI
29. Yang, M.; Gong, K.; Cui, Y.; Liu, S.; Li, G.; Lin, S. Band engineering and structural-geometrical engineering in 2D/3D van der Waals heterostructures for advanced photodetection and intelligent sensing. *Nano-Micro. Lett.* **2026**, *18*, 298. DOI PubMed PMC
30. Liu, M.; Su, H.; Liu, X.; et al. Dynamic modulation of electron redistribution at the heterogeneous interface nickel hydroxides/platinum boosts acidic oxygen reduction reaction. *Nat. Commun.* **2025**, *16*, 2826. DOI PubMed PMC
31. Li, G.; Deng, F.; Ma, T.; et al. Integrating Ni_2P crystalline-NiFeBP amorphous heterojunction nanosheets on hierarchical nickel foam for superior overall water splitting. *Chem. Eng. J.* **2025**, *505*, 159290. DOI
32. Li, J.; Peng, X.; Liu, Z.; Tian, Y.; Wang, C. Defect-rich Zn_2SnO_x/SnO_x heterostructure for high sulfur utilization and uniform Li^+ transport toward stable Li-S full batteries. *Nano. Res.* **2026**, *19*, 94908323. DOI
33. Zhang, W.; Li, L.; Wang, Q.; et al. Electrochemical performance of MoB/Si_3N_4 Heterojunction as a potential anode material for Li ion batteries. *ACS. Appl. Mater. Interfaces.* **2024**, *16*, 62155-70. DOI
34. Aravind, A. M.; Tomy, M.; Kuttapan, A.; Kakkassery Aippunny, A. M.; Suryabai, X. T. Progress of 2D MXene as an electrode architecture for advanced supercapacitors: a comprehensive review. *ACS. Omega.* **2023**, *8*, 44375-94. DOI PubMed PMC
35. Zang, S.; Hu, C.; Nie, L.; et al. Research progress in anode materials based on multiple potassium storage mechanisms. *Sustainable. Mater. Technol.* **2022**, *33*, e00480. DOI
36. Ye, J.; Wang, Z.; Liu, Q.; et al. Rational design of a setaria-like $NiTe_2$/MoS_2 semi-coherent heterogeneous interface for enhancing diffusion kinetics in potassium-ion batteries. *J. Colloid. Interface. Sci.* **2024**, *674*, 527-36. DOI
37. Zhang, Y.; Liu, L.; Zhao, L.; et al. Sandwich-like $CoMoP_2$/MoP heterostructures coupling N, P co-doped carbon nanosheets as advanced anodes for high-performance lithium-ion batteries. *Adv. Compos. Hybrid. Mater.* **2022**, *5*, 2601-10. DOI
38. Ye, Y.; Chen, M.; Liu, S.; et al. Enhanced built-in electric field facilitates electron and ion transfer for high-performance lithium-sulfur batteries. *ACS. Sustainable. Chem. Eng.* **2025**, *13*, 20253-64. DOI
39. Liu, S.; Chen, M.; Luo, Y.; et al. Synergistic electrochemical catalysis by high-entropy metal phosphide in lithium-sulfur batteries. *J. Colloid. Interface. Sci.* **2024**, *669*, 126-36. DOI
40. Lai, C.; Chen, K.; Lei, M.; Hu, J.; Chen, S.; Li, C. Highly reversible iron fluoride conversion cathodes enabled by deep-eutectic solvent method and heterostructure design. *Adv. Funct. Mater.* **2024**, *34*, 2312415. DOI

41. Xue, Y.; Luo, D.; Yang, N.; et al. Engineering checkerboard-like heterostructured sulfur electrocatalyst towards high-performance lithium sulfur batteries. *Chem. Eng. J.* **2022**, *440*, 135990. DOI
42. Zhang, W.; Li, L.; Ren, J.; et al. Heterojunction engineering of conductive ability and structural stability for the electrochemical performance of MoB anode material. *Journal. of. Energy. Storage.* **2025**, *112*, 115589. DOI
43. Zuo, X.; Qiu, Y.; Zhen, M.; Liu, D.; Zhang, Y. Review on MXenes-based electrocatalysts for high-energy-density lithium-sulfur batteries. *Nano-Micro. Lett.* **2025**, *17*, 209. DOI
44. Javed, M. S.; Zhang, X.; Ali, S.; et al. Heterostructured bimetallic-sulfide@layered $Ti_3C_2T_x$-MXene as a synergistic electrode to realize high-energy-density aqueous hybrid-supercapacitor. *Nano. Energy.* **2022**, *101*, 107624. DOI
45. Shah, S. A.; Pato, A. H.; Jangra, S.; et al. Emerging MXene/metal selenides for energy solutions: A comprehensive review. *Nano. Research.* **2025**, *18*, 94907855. DOI
46. Zhang, N.; Meng, Q.; Wu, H.; et al. Co-MOF as stress-buffered architecture: an engineering for improving the performance of NiS/SnO_2 heterojunction in lithium storage. *Adv. Energy. Mater.* **2023**, *13*, 2300413. DOI
47. Lan, X.; Yang, S.; Meng, T.; Zhang, C.; Hu, X. A multifunctional electrolyte additive with solvation structure regulation and electrode/electrolyte interface manipulation enabling high-performance Li-ion batteries in wide temperature range. *Adv. Energy. Mater.* **2023**, *13*, 2203449. DOI
48. Wang, C.; Zhang, Z.; Zheng, Y.; et al. Constructing face-shared configuration at the hetero-interface in Li-rich layered oxide cathodes. *Angew. Chem. Int. Ed.* **2026**, *65*, e2943336. DOI
49. Yu, R.; Wang, G.; Wu, B.; et al. Synergistic energy band modulation and interfacial structure engineering for highly-reversible anionic redox in Li-rich Mn-based layered oxides. *Energy. Storage. Mater.* **2025**, *80*, 104447. DOI
50. Zhu, Y.; Gu, J.; Zhang, G.; et al. A Si-$MoSe_2$ heterostructured anode with enhanced thermal transport and electrochemical performance for liquid and all-solid-state lithium-ion batteries. *Adv. Sci.* **2026**, *13*, e23320. DOI
51. Liu, M.; Guan, Z.; Zheng, L.; et al. Layered-to-rocksalt atomic reconfiguration on O3-type cathodes surface for high-energy and durable sodium-ion batteries. *Mater. Today.* **2025**, *89*, 35-43. DOI
52. Geng, J.; Sun, C.; Xie, J.; et al. Topological transformation construction of a $CoSe_2$/N-doped carbon heterojunction with a three-dimensional porous structure for high-performance sodium-ion half/full batteries. *Inorg. Chem. Front.* **2022**, *9*, 3176-86. DOI
53. Chen, X.; Zeng, J.; Wu, J.; et al. Air stability and Na site activation of NASICON-based NFPP/NVOPF/C heterostructured cathode via surface reconstruction. *Adv. Funct. Mater.* **2025**, *36*, e11174. DOI
54. Zhang, M.; Wang, S.; Zhu, J.; et al. Optimized heterostructures by preferred crystal orientation for ultrafast sodium storage. *Adv. Funct. Mater.* **2025**, *35*, 2500165. DOI
55. Jiang, Y.; Lian, M.; Ma, J.; et al. Synchronous regulation of S-deficient ZnS-MoS_2 heterostructure nanoreactor for fast and durable sodium storage. *Nano. Lett.* **2025**, *25*, 7241-8. DOI
56. Song, L.; Zhang, S.; Duan, L.; et al. Tunable interfacial electric field-mediated cobalt-doped FeSe/Fe_3Se_4 heterostructure for high-efficiency potassium storage. *Angew. Chem. Int. Ed.* **2024**, *63*, e202405648. DOI
57. Wang, T.; Li, M.; Qi, L.; Jie, P.; Yang, W.; Li, Y. Multilevel heterostructure of MoS_2/GDYO for lithium-ion batteries. *Adv. Funct. Mater.* **2023**, *33*, 2308470. DOI
58. Li, M.; Wang, C.; Wang, C.; et al. 10 years development of potassium-ion batteries. *Adv. Mater.* **2025**, *37*, 2416717. DOI
59. Jia, X.; Chen, H.; Sun, H.; Zhu, J.; Lu, B. Promoting robust potassium storage via engineered Zn-S bond. *Adv. Energy. Mater.* **2025**, *15*, 2501487. DOI
60. Wang, X.; Zhao, J.; Chen, Y.; et al. Yolk-shell MnSe/ZnSe heterostructures with selenium vacancies encapsulated in carbontubes for high-efficiency sodium/potassium Storage. *Small* **2023**, *20*, 2307747. DOI
61. Li, Q.; Liang, Z.; Huang, Y.; et al. Tailoring self-catalytic N-Co bonds into heterostructure architectures: deciphering polytellurides conversion mechanism toward ultralong-lifespan potassium ion storage. *Adv. Mater.* **2025**, *37*, 2502894. DOI
62. Wang, T.; He, J.; Zhu, Z.; et al. Heterostructures regulating lithium polysulfides for advanced lithium-sulfur batteries. *Adv. Mater.* **2023**, *35*, 2303520. DOI
63. Hu, Y.; Chen, W.; Lei, T.; et al. Strategies toward high-loading lithium-sulfur battery. *Adv. Energy. Mater.* **2020**, *10*, 2000082. DOI
64. Wang, T.; Tan, X.; Ma, Y.; Ma, Y.; Wu, Y. High-entropy materials regulating lithium polysulfides for advanced lithium-sulfur batteries. *Chem. Eng. J.* **2025**, *519*, 165580. DOI
65. Wang, T.; Zhong, J.; Huang, X.; et al. Highly synergistic electrocatalysis and confinement of covalently bonded heterostructures enable high-efficient-stable Li-S batteries. *Energy. Storage. Mater.* **2025**, *81*, 104477. DOI
66. Wang, T.; He, J.; Cheng, X.; Zhu, J.; Lu, B.; Wu, Y. Strategies toward high-loading lithium-sulfur batteries. *ACS. Energy. Lett.* **2022**, *8*, 116-50. DOI

67. Song, H.; Nguyen, T. T.; Chu, R.; Bai, Y.; Kim, N. H.; Lee, J. H. Coupling interfacial effect in heterogeneous RuP_2-RuP for accelerating sulfur reduction reaction of lithium sulfur batteries. *Nano. Energy.* **2024**, *128*, 109859. DOI
68. Jiao, X.; Tan, L.; Tang, X.; et al. A 405 W h kg^{-1} Ah-level lithium-sulfur pouch battery stabilized over 200 cycles by an electron-triode-like GeS_2-NiS_2 heterostructure. *Energy. Environ. Sci.* **2025**, *18*, 4053-67. DOI
69. Chen, B.; He, C.; Tao, Y.; et al. Lattice-confined single-atom Fe tunes co spin states for fast sulfur redox in Li S batteries. *Chem. Eng. J.* **2025**, *525*, 170280. DOI
70. Huang, C.; Yu, J.; Zhang, C. Y.; et al. Electronic spin alignment within homologous NiS_2/$NiSe_2$ heterostructures to promote sulfur redox kinetics in lithium-sulfur batteries. *Adv. Mater.* **2024**, *36*, 2400810. DOI
71. Yu, S.; Yin, L.; Zhang, C.; et al. Asymmetric cobalt sites induced low-spin state for enhanced redox kinetics in lithium-sulfur batteries. *eScience* **2026**, 100552. DOI
72. Liu, Y.; Li, L.; Li, X.; et al. Asymmetric tacticity navigates the localized metal spin state for sustainable alkaline/sea water oxidation. *Sci. Adv.* **2025**, *11*, eads0861. DOI PubMed PMC
73. Wang, T.; Yao, H.; Luo, Z.; et al. Interface-regulated bifunctional separator for highly robust lithium sulfur batteries. *Mater. Today.* **2026**, *97*, 103363. DOI
74. Wu, G.; Fan, Y.; Li, J.; et al. Facilitated polysulfide redox conversion by delocalized electrons in MBene heterointerface for highly stable lithium-sulfur batteries. *Nano-Micro. Lett.* **2026**, *18*, 252. DOI
75. Wang, T.; Shi, Z.; Xu, B.; et al. A thermally conductive separator for safe lithium metal batteries. *ACS. Energy. Lett.* **2026**, *11*, 3880-9. DOI
76. Hao, M.; Xiong, X. G.; Li, Z.; et al. Adsorption-catalysis synergy boosting the conversion of polysulfide over mesoporous carbon confined molecular catalysts. *Adv. Energy. Mater.* **2025**, *15*, 2501226. DOI
77. Ma, C.; Zhao, S.; Chen, H.; et al. Intimate heterostructured electrocatalyst for functional tandem catalysts of lithium polysulfides in separator-modified lithium-sulfur batteries. *Carbon. Energy.* **2025**, *7*, e70033. DOI
78. Xu, G.; Song, X.; Jiang, M.; Wang, R.; Lian, S.; Yang, X. Synergistic promotion of reaction kinetics for LiPSs at high loadings by interfacial built-in electric field and sulfur vacancies of ternary heterostructure for high-performance Li-S batteries. *Appl. Catal. B. Environ.* **2025**, *362*, 124707. DOI
79. Feng, J.; Li, Z.; Zhao, L.; et al. Built-in electric field and Te charge modulation in 2D Bi_2Te_3@Sb_2Te_3 heterostructure enable ultralong cycling for lithium-air batteries. *Adv. Funct. Mater.* **2025**, *35*, 2504803. DOI
80. Sun, C.; Xiao, F.; Li, M.; et al. Partial-oxidation enabling homologous Ru/RuO_2 heterostructures with proper d-dand center as efficient and durable cathode catalysts for ultralong cycle life in Li-O_2 batteries. *Adv. Energy. Mater.* **2024**, *15*, 2402699. DOI
81. Zhu, T.; Xia, C.; Wu, B.; et al. Inbuilt photoelectric field of heterostructured cobalt/iron oxides promotes oxygen electrocatalysis for high-energy-efficiency zinc-air batteries. *Appl. Catal. B. Environ.* **2024**, *357*, 124315. DOI
82. Xia, Y.; Wang, L.; Gao, G.; et al. Constructed Mott-Schottky heterostructure catalyst to trigger interface disturbance and manipulate redox kinetics in Li-O_2 battery. *Nano-Micro. Lett.* **2024**, *16*, 258. DOI
83. Lu, Z.; Wang, Z.; Yang, Z.; et al. Engineering CoN_4 and FeN_4 dual sites with adjacent nanoclusters on flexible porous carbon fibers for enhanced electrocatalytic oxygen reduction and evolution. *Adv. Funct. Mater.* **2024**, *35*, 2418489. DOI
84. Zhang, J.; Dong, X.; Wang, G.; Chen, J.; Wang, R. Interfacial engineering-induced Janus heterostructures with enhanced electronic regulation for efficient oxygen electrocatalysis in rechargeable Zn-air batteries. *Appl. Catal. B-Environ.* **2024**, *342*, 123459. DOI
85. Xu, Z.; Chen, J.; Zhang, T.; et al. Enhancing efficiency and durability of alkaline Zn-Co/air hybrid batteries with self-reconstructed Co/Co_2P heterojunctions. *Adv. Energy. Mater.* **2024**, *15*, 2402839. DOI
86. Xu, Z.; Wu, J.; Chen, W.; et al. Plasma-assisted nitridation modulates the electronic structure of the $NiSe_2$/Ni@Ni_3N ternary heterojunction enhancing its dual-function catalytic performance and inhibiting zn dendrite growth in rechargeable zinc-air batteries. *Adv. Funct. Mater.* **2025**, *35*, e11117. DOI
87. Zhang, S.; Chen, Q.; Zheng, L.; et al. Heteroengineered Fe_2N/CrN_x with accelerated proton-coupled electron transfer for efficient oxygen reduction in aluminum-air batteries. *Adv. Mater.* **2025**, *38*, e14607. DOI
88. Wu, M.; Zhan, X.; Yang, S.; et al. The $2e^-$ *vs.* $4e^-$ pathways for ORR in rechargeable zinc-air batteries. *Energy. Environ. Sci.* **2026**, *19*, 1899-915. DOI
89. Wan, Y.; Pei, M.; Tang, Y.; et al. Interfacial water regulation for nitrate electroreduction to ammonia at ultralow overpotentials. *Adv. Mater.* **2025**, *37*, 2417696. DOI
90. Sun, S.; Huang, W.; Yu, H.; Sun, Z.; Shang, W.; Wen, Y. Constructing MXene@ZIF-67 core-shell heterostructures on mg anodes for a high-performance aqueous Mg battery. *J. Alloys. Compd.* **2025**, *1016*, 178899. DOI

91. Yang, M.; Chuai, M.; Lai, M.; et al. Customizable crystalline-amorphous rectifying heterostructure cathodes for durable and super-fast zinc storage. *Energy. Environ. Sci.* **2025**, *18*, 4651-64. DOI
92. Zheng, Z.; Ding, C.; Hasan, M. S.; et al. *In-situ* study of photo-rechargeable aqueous zinc-ion batteries with the bifunctional α-MnO_2Photoelectrodes. *Adv. Funct. Mater.* **2025**, *35*, 2500182. DOI
93. Zhao, X.; Zhang, F.; Li, H.; et al. Dynamic heterostructure design of MnO_2 for high-performance aqueous zinc-ion batteries. *Energy. Environ. Sci.* **2024**, *17*, 3629-40. DOI
94. Wang, T.; Wang, C.; Silva, G. V. D. O.; et al. Electrode interface engineering of hydrophilic and zincophilic bifunctionality for high-efficiency and low-polarization Zn anodes. *Adv. Funct. Mater.* **2024**, *34*, 2408662. DOI
95. Chen, M.; Zhou, M.; Wang, Q.; et al. Desolvation effect triggered by TiS_2-TiO_2 heterostructure for ultrahigh-rate aqueous zinc-ion batteries. *Adv. Funct. Mater.* **2024**, *35*, 2414032. DOI
96. Fu, Y.; Zhong, J.; Zhang, S.; et al. Interfacial electronic nanoarchitectonics for sustainable Zn-I_2 batteries. *Angew. Chem. Int. Ed.* **2026**, *65*, e22065. DOI
97. Jia, B.; Hu, E.; Hu, Z.; et al. Laminated tin-aluminum anodes to build practical aqueous aluminum batteries. *Energy. Storage. Mater.* **2024**, *65*, 103141. DOI
98. Yang, Z.; Cheng, H.; Yang, W.; et al. Local microenvironment-induced dynamic self-adaptation for high-performance ammonium-ion batteries. *ACS. Nano.* **2025**, *19*, 37154-64. DOI
99. Ran, Q.; Shi, H.; Meng, H.; et al. Aluminum-copper alloy anode materials for high-energy aqueous aluminum batteries. *Nat. Commun.* **2022**, *13*, 576. DOI PubMed PMC
100. Kulkarni, A.; Dandriyal, A.; Patil, S.; et al. Spinel-structured tetragonal Mn_3O_4 nanocrystals as promising electrode for aqueous ammonium-ion storage. *Energy. Storage. Materials.* **2026**, *86*, 105029. DOI